



Article

Potent Alkaline Phosphatase Inhibitors, Pyrazolo-Oxothiazolidines: Synthesis, Biological Evaluation, Molecular Docking, and Kinetic Studies

Narges Hosseini Nasab ¹, Hussain Raza ¹ , Rok Su Shim ¹, Mubashir Hassan ², Andrzej Kloczkowski ² and Song Ja Kim ^{1,*}

¹ Department of Biological Sciences, Kongju National University, Gongju 32588, Chungnam, Korea

² Department of Pediatrics, The Steve and Cindy Rasmussen Institute for Genomic Medicine at Nationwide Children's Hospital, Columbus, OH 43205, USA

* Correspondence: ksj85@kongju.ac.kr

Abstract: To develop new alkaline phosphatase inhibitors (ALP), a series of pyrazolo-oxothiazolidine derivatives were synthesized and biologically assessed, and the results showed that all of the synthesized compounds significantly inhibited ALP. Specifically, compound **7g** displayed the strongest inhibitory activity ($IC_{50} = 0.045 \pm 0.004 \mu\text{M}$), which is 116-fold more active than monopotassium phosphate ($IC_{50} = 5.242 \pm 0.472 \mu\text{M}$) as a standard reference. The most potent compound among the series (**7g**) was checked for its mode of binding with the enzyme and shown as non-competitively binding with the target enzyme. The antioxidant activity of these compounds was examined to investigate the radical scavenging effect. Moreover, the MTT assay method was performed to evaluate their toxic effects on the viability of MG-63 human osteosarcoma cells, and all compounds have no toxic effect on the cells at $4 \mu\text{M}$. Computational research was also conducted to examine the binding affinity of the ligands with alkaline phosphatase, and the results revealed that all compounds showed good binding energy values within the active site of the target. Therefore, these novel pyrazolo-oxothiazolidine derivatives might be employed as promising pharmacophores for potent and selective alkaline phosphatase inhibitors.

Keywords: pyrazolo-oxothiazolidine; alkaline phosphatase; kinetic analysis; cell viability; molecular docking



Citation: Hosseini Nasab, N.; Raza, H.; Shim, R.S.; Hassan, M.; Kloczkowski, A.; Kim, S.J. Potent Alkaline Phosphatase Inhibitors, Pyrazolo-Oxothiazolidines: Synthesis, Biological Evaluation, Molecular Docking, and Kinetic Studies. *Int. J. Mol. Sci.* **2022**, *23*, 13262. <https://doi.org/10.3390/ijms232113262>

Academic Editor: Alexander Y. Tsygankov

Received: 27 September 2022

Accepted: 28 October 2022

Published: 31 October 2022

Publisher's Note: MDPI stays neutral with regard to jurisdictional claims in published maps and institutional affiliations.



Copyright: © 2022 by the authors. Licensee MDPI, Basel, Switzerland. This article is an open access article distributed under the terms and conditions of the Creative Commons Attribution (CC BY) license (<https://creativecommons.org/licenses/by/4.0/>).

1. Introduction

Alkaline phosphatases [ALP; orthophosphoric monoester phosphohydrolase (alkaline optimum) EC 3.1.3.1], which are widely distributed in nature from prokaryotes and higher eukaryotes to humans [1,2], are known as plasma membrane-bound glycoproteins [3,4]. Alkaline phosphatase belongs to a large family of dimeric enzymes that hydrolyzes various monophosphate esters at a high pH optimum with the release of inorganic phosphate [5,6]. It is often restricted to the cell surface [7,8]. ALP, as a representative mediator of biochemistry, actively participates in most biological processes, including metabolism, signal transduction, molecular transport, and the manifestation of genetic information. ALP has a catalytic function because of its structural composition, which consists of two monomers with five cysteine residues, two zinc atoms (Zn^{2+}), and one magnesium atom (Mg^{2+}) in each monomer [9–11]. The ALP monomer's conformation is significantly affected by these metal ions, and they also indirectly adjust interactions between subunits [12]. Human ALPs can be divided into at least four isoenzymes, depending on the specificity of the tissue that will express them. Three of them are tissue-specific enzymes including placental alkaline phosphatase (PLALP or Regan isozyme), intestinal alkaline phosphatase (IALP), and germ cell ALP (GCALP or NAGAO isozyme), while the fourth is tissue nonspecific enzyme as liver/bone/kidney alkaline phosphatase (L/B/K ALP) [13]. By performing inorganic pyrophosphate (PPi) hydrolysis, L/B/K ALP maintains an optimum pyrophosphate level in bone tissues. The intestinal ALPs are

present in the epithelial linings of the intestine and regulate the detoxification of bacterial lipopolysaccharides, bicarbonate secretion, and lipid intestinal absorption. Certain amino acids inhibit ALPs in a non-competitive manner. L-phenylalanine inhibits the tissue-specific isozymes (PLALP, GCALP, and IALP) 30 times more sensitively than the L/B/K ALPs, whereas the L/B/K ALPs are more sensitive to inhibition by L-homoarginine (Har) than PLALP, GCALP, and IALP. *r*-Phenylalanyl-glycyl-glycine (Pgg) gives strong differential inhibition between PLALP, IALP, and L/B/K ALPs. Levamisole (Leva) is a highly effective inhibitor of L/B/K ALP but has a minor inhibitory impact on the other ALPs [14].

Numerous disorders, including bowel diseases, sepsis, arthritis, multiple sclerosis, atherosclerosis, and esophageal, breast, liver, intestinal, prostate, ovarian, and intestinal cancers are also associated with the overexpression of IALPs [15–17]. The elevated expression of ALP in cancer patients indicates metastasis to the liver and bone. Hepatocellular carcinomas have been discovered to have higher IALP levels [18], while osteosarcomas, breast cancer, and osteoblastic bone metastasis have all been associated with increased plasma levels of L/B/K ALP [19]. Moreover, some metabolic disorders such as Wilson's disease or hematological diseases such as aplastic anemia and chronic myelogenous leukemia have occurred when ALP concentration is at its low level [20]. The investigation for efficient and selective ALP isozyme inhibitors is becoming more popular. In recent years, various ALP inhibitors have been reported based on biaryl sulfonamide, chromone, triazole, and coumarin sulfonate motifs [21]. Some compounds were discovered to be efficient ALP inhibitors; however, the majority of them inhibited ALPs non-selectively [22–24]. Traditionally, the only ALP inhibitors available were levamisole and theophylline, with K_i values of 16 and 82 μM , respectively [25]. However, in order to comprehend the role of ALPs in health and disease, it is imperative to develop small drug-like molecules as efficient and selective inhibitors of ALP isozymes. Figure 1 demonstrates some identified representative ALP inhibitors [26,27]. As a result, ALPs represent an attractive molecular target for drug discovery, and the development of effective and selective ALP isozyme inhibitors is desperately required.

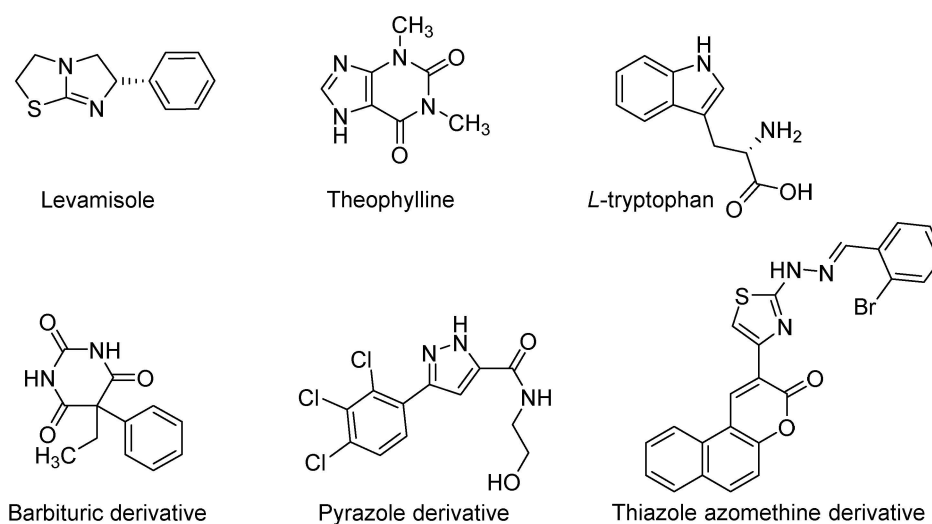


Figure 1. Identified inhibitors of ALP.

Heterocyclic compounds have a cyclic structure in which the ring contains two or more different types of atoms. Also, a large number of heterocyclic compounds are known, and the number is continually growing. Heterocycles are well-studied bioactive compounds and thought to be attractive synthetic targets for the creation of new therapeutics [28]. One important topic for organic chemists is the synthesis of various heterocyclic compounds from straightforward and easily accessible starting materials [29–32].

Pyrazoles are a five-membered aromatic heterocyclic system from the azole branch with two adjacent nitrogen atoms. They are a significant class of heterocyclic compounds that have a variety of chemical, biological, agrochemical, and pharmacological activities [33].

In medicinal chemistry, compounds possessing pyrazole rings have shown biological activity, including antimicrobial [34,35], antifungal [34], leishmanicidal [36,37], antiviral [35], antichagasic [38], pesticidal [39], antihyperglycemic [40], anti-inflammatory [41], and antitumoral [35] activities. Similarly, it has been established that thiazolidinones, a type of five-membered heterocyclic compounds that include sulfur at position 1, nitrogen at position 3, and a carbonyl group at position 4, have significant biological activities. Its derivatives are among the most broadly investigated moieties, and the first recognition of its natural occurrence was its existence in penicillin [42]. In several fields, including chemistry, pharmacology, biology, and materials science, they have a broad spectrum of applications [43]. Thiazolidinone have biological effects such as anticonvulsant [44], hypnotic [45], antitubercular [46], antibacterial [47], anticancer [48], and anti-inflammatory [49] properties.

A modern concept in drug development is the use of pharmacophore hybrids to create compounds that have superior affinity and efficacy [50]. In considering the aforementioned facts, a reasonable and promising area of research in current medicinal chemistry is the design of novel small molecules with drug-like properties based on the pharmacologically attractive scaffolds of pyrazole and thiazolidinones [50]. Some recent synthetic studies of pyrazole–thiazolidines and related hybrids, along with their biological investigations, have been patented as necroptosis inhibitors [51], VHR protein tyrosine phosphatase inhibitors [52], Pin1-modulating compounds [53], and RNA-binding protein modulators [54]. The pyrazole–thiazolidinone hybrids were investigated for their ability to inhibit the TNF- α -TNFRc1 interaction [55], histone acetyltransferases inhibitors [56], COX inhibitors [57], and ADAMTS-5 enzymes [58].

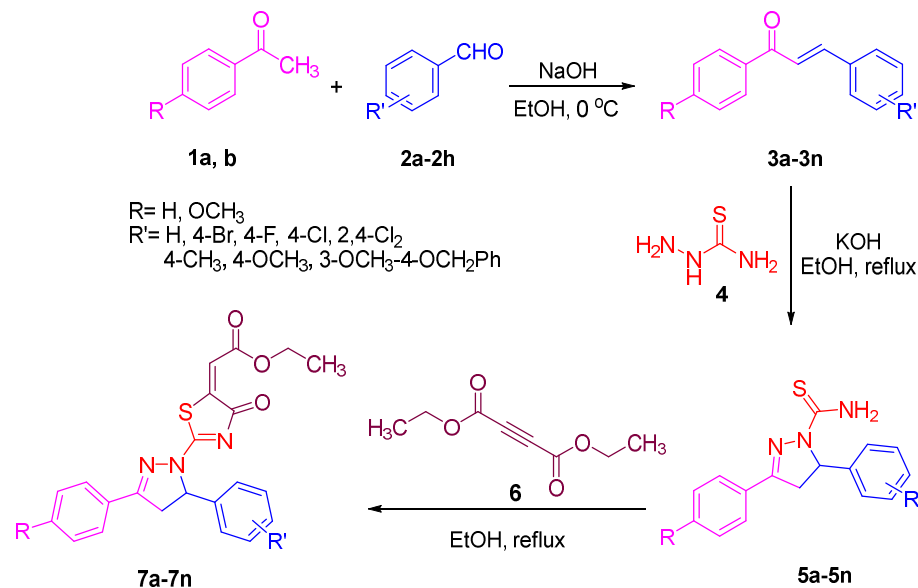
As a result, in accordance with previously reported alkaline phosphatase inhibitors (Figure 1), we combined two scaffolds (pyrazole and thiazolidinone) to create a novel scaffold that was used in the ALP inhibition investigation. Moreover, to the best of our knowledge, pyrazolo-oxothiazolidine derivatives have never been researched as alkaline phosphatase inhibitors. Here, we described the design and synthesis of a novel class of ALP inhibitory agents which were also evaluated for antioxidant activity, cytotoxicity, and computational studies.

2. Results and Discussion

2.1. Chemistry

According to Scheme 1, a new series of pyrazolo-oxothiazolidine derivatives was synthesized in three steps. Initially, the Claisen–Schmidt condensation of acetophenone or *para*-methoxy acetophenone (**1a**, **b**) and aromatic aldehydes (**2a–2h**) in the presence of sodium hydroxide in ethanol resulted in 1,3-diphenylprop-2-en-1-ones (chalcones, **3a–3n**). Then, the intermolecular cyclization of different chalcone derivatives (**3a–3n**) with thiosemicarbazide (**4**) produced pyrazole compounds (**5a–5n**) in refluxing ethanol under basic conditions. Finally, the reaction of compounds **5a–5n** and diethyl acetylenedicarboxylate (**6**) is accomplished under reflux conditions in ethanol, to form pyrazolo-oxothiazolidine derivatives (**7a–7n**) in reasonable yields (80–92%). The structural confirmation of all synthesized compounds (**7a–7n**) was verified through the spectroscopic analysis utilizing FT-IR, ^1H NMR, and ^{13}C NMR. To comprehend the structural identification of the synthesized target compounds, we have presented a structural interpretation of one of the target compounds (**7a**). Molecule **7a** was obtained in 84% yield as a white solid with a melting point of 242–244 °C. FT-IR spectroscopy was used to examine the molecular vibrational studies to confirm various functionalities. The aliphatic C-H stretching vibrations were observed at 2974 cm^{-1} . The stretching bands for conjugated C=O group appeared at 1694 cm^{-1} . The other significant absorption bands in the IR spectrum emerged at 1602 (C=C, alkene), 1548, 1498 (C=C, aromatic), 1489 (C=N, stretching), 1218 (C-O, stretching), 1177, 1114, 1073, 1010 (C-N stretching and aromatic C-H out of plane bending), 823, 767, 757 (aromatic C-H out of plane bending), 689 (C-Br stretching), which prove the existence of functional groups such as pyrazole, ester, alkene, and aromatic in this molecule. The number of proton-containing atoms in the produced molecules was measured using ^1H NMR spectroscopic techniques.

There are two phenyl rings in the target compound **7a**. In the aromatic region, the two multiplet peaks at δ 7.14–7.18 (m, 2H, H-13 & 17), and 7.83–7.85 (m, 2H, H-14 & 16) belonged to the aromatic ring which holds the bromo group at the *para* position, whereas five protons of second phenyl ring represented by multiplet at δ 7.46–7.58 (m, 5H, H-1, 2, 3, 4 & 6). In the up-field region of the spectrum, the signals at δ 1.37 (t, J = 8 Hz, 3H, CH₃) and 4.34 (q, J = 7.2 Hz, 2H, CH₂), exposed the presence of methyl and methylene groups, which split triplet and quartet, respectively. At δ 6.93 (s, 1H, H-24), there was a distinct singlet signal for vinylic hydrogen. The typical ABX system, which is associated with the CH₂ and CH protons of the pyrazoline ring, was clearly detected in the predicted regions. The H_A proton was observed at δ 3.43 (dd, J = 18, 4 Hz, 1H, H-8_A), the H_B proton appeared at δ 4.03 (dd, J = 18, 12 Hz, 1H, H-8_B), and the H_X emerged at 5.85 (dd, J = 11.2, 4 Hz, 1H, H-9), due to vicinal coupling with two magnetically non-equivalent protons of the methylene group at position 4 of the pyrazoline ring. Furthermore, the carbon backbone of the produced target compound **7a** was studied using the ¹³C NMR technique. Due to some duplets for magnetically equivalent carbons that reduced the total number of resonances in the molecule, the ¹³C NMR spectra showed a total of eighteen carbon resonances. Two resonances for the phenyl ring which holds the bromo group at the *para* position were observed at δ 127.68 (C-13 & C-17) and 132.39 (C-14 & C-16), while another phenyl ring emerged at δ 127.52 (C-4 & C-6), 129.11 (C-1 & C-3), and 129.43 (C-2). The two carbonyl carbons (C-25) and (C-20) appeared at δ 166.59 and 173.81 ppm, whereas two imine carbons (C-7) and (C-18) were observed at δ 160.79 and 178.68 ppm. Four quaternary signals were characterized at δ 122.65 (C-15), 132.16 (C-5), 138.15 (C-12), and 146.52 (C-21). One signal at δ 118.17 ppm belonged to the methine carbon (C-24). There were four peaks in the aliphatic region that were distinguished by the methyl and methylene carbons at positions 14.23 (C-29), 43.30 (C-8), 61.75 (C-28), and 63.38. (C-9) (Figure 2).



Scheme 1. General synthesis of novel pyrazolo-oxothiazolidine derivatives (**7a–7n**).

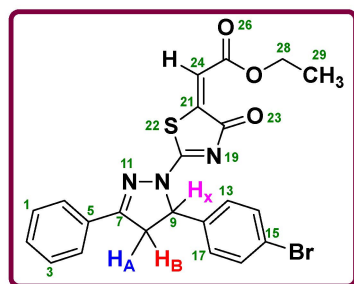


Figure 2. ABX system of the pyrazoline ring.

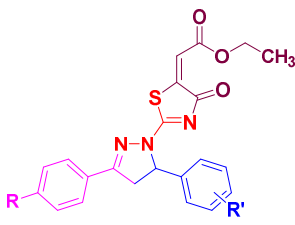
2.2. Biological Evaluations

2.2.1. Alkaline Phosphatase Activity and Structural Activity Relationship (SAR)

The synthesized chemical compounds (**7a–7n**) were evaluated against the calf intestinal alkaline phosphatase (CIAP) enzyme inhibition for the IC_{50} evaluation. Table 1 gives an overview of the CIAP results. Monopotassium phosphate (KH_2PO_4) was employed in this experiment as a positive control to evaluate the performance of our synthetic compounds. Interestingly, all these compounds showed extremely strong inhibitory activity against this enzyme, as evidenced by their lower IC_{50} (0.045–2.987 μM) values in comparison to the standard reference KH_2PO_4 , which had an IC_{50} value of $5.242 \pm 0.472 \mu M$. Though the observed activity is the resultant of the entire molecule, the effect of various aryl groups on the inhibitory potential allowed for the recognition of a limited structure-activity relationship (SAR). To make the classification of the structure activity relationship (SAR) more understandable, we divide it into three categories. The first five compounds **7(a–d)**, and **7l**, while having the unsubstituted phenyl ring scaffold, differ in their second phenyl ring derivatives. It observed that compounds **7a** and **7l**, which have halogen groups (Br and Cl) at the *para* position, showed better activity when compared to other derivatives (**7b**, **7c**, **7d**), which have electron-donating groups at the *para* position. However, a reverse trend was noticed in the second set of seven compounds **7e**, **7f**, **7g**, **7h**, **7i**, **7k**, and **7m**, which all possess a *para*-methoxy phenyl ring, and the second phenyl ring has various derivatives. Among halogenated molecules (**7h**, **7m**, **7f**, and **7i**), compound **7h** with bromo group at *para* position exhibited less activity probably because a bulky bromo group decreases the inhibitory activity. Compound **7f** with chloro group at *ortho* and *para* position showed lower inhibitory potential as compared to **7m** in which chloro group was at *para* position, and presumably due to steric crowding prevents the good interaction with the active site of the enzyme. Compounds **7i** and **7m**, which have fluoro and chloro groups in the *para* positions, respectively, displayed a similar inhibitory effect. Additionally, the methyl, methoxy-benzyloxy, and methoxy groups found in compounds **7e**, **7g**, and **7k** in this category showed overall the strongest inhibitory potentials against the target enzyme. So, it can be concluded that, when one phenyl ring has a *para*-methoxy group, the electron-withdrawing groups significantly disrupted the electronic density of the aromatic ring, and more effective interactions are made by electron-donating substances with the enzyme. Surprisingly, the most effective molecule **7g** ($IC_{50} = 0.045 \pm 0.004 \mu M$) comprised both benzyloxy and methoxy groups, which showed synergistic effects. This might be caused by the ability of both groups to donate electrons via resonance and created more hydrogen bonds. Finally, between compounds **7n** and **7j**, compound **7j** ($IC_{50} = 0.434 \pm 0.011 \mu M$) with only one methoxy group at *para* position showed almost six-fold better inhibitory potential compared to **7n** ($IC_{50} = 2.987 \pm 0.734 \mu M$) having unsubstituted phenyl rings. It means that compared to an unsubstituted compound, the presence of an electron-donating substituent on the phenyl group makes the molecule a more suitable inhibitor. Overall, all of the derivatives have noticeable inhibitory activity, particularly compound **7g** possessing the strongest effect compared to reference standard. As a consequence of these findings, it can be concluded that phenyl rings need to contain electron-rich species like methoxy

and benzyloxy groups in order to have alkaline phosphatase inhibitory activity. Therefore, compound **7g** could be a perfect choice for medicinal purposes.

Table 1. Alkaline phosphatase inhibitory activity of pyrazolo-oxothiazolidine derivatives (**7a–7n**).



7a-7n

No.	Compound	R	R'	Alkaline Phosphatase IC ₅₀ ± SEM (μM)
1	7a	H	4-Br	0.053 ± 0.001
2	7b	H	4-CH ₃	2.298 ± 0.151
3	7c	H	4-OCH ₃	0.198 ± 0.018
4	7d	H	3-OCH ₃ -4-OCH ₂ C ₆ H ₅	0.293 ± 0.039
5	7e	OCH ₃	4-CH ₃	0.228 ± 0.012
6	7f	OCH ₃	2,4-Cl ₂	0.566 ± 0.048
7	7g	OCH₃	3-OCH₃-4-OCH₂C₆H₅	0.045 ± 0.004
8	7h	OCH ₃	4-Br	0.907 ± 0.041
9	7i	OCH ₃	4-F	0.315 ± 0.017
10	7j	OCH ₃	H	0.434 ± 0.011
11	7k	OCH ₃	4-OCH ₃	0.075 ± 0.005
12	7l	H	4-Cl	0.051 ± 0.019
13	7m	OCH ₃	4-Cl	0.302 ± 0.004
14	7n	H	H	2.987 ± 0.734
15		KH₂PO₄		5.242 ± 0.472

Values are presented as mean ± SEM (Standard error of the mean).

2.2.2. Kinetic Mechanism for CIAP

Presently, the most active compound **7g** was considered for the mode of inhibition of CIAP. The capacity of the compound to inhibit the free enzyme and enzyme-substrate complex was determined in terms of EI and ESI constants, respectively. The kinetic research of the enzyme by the Lineweaver–Burk plot of $1/V$ versus substrate $p\text{-NPP } 1/[S]$ in the presence of different inhibitor concentrations gave a series of straight lines as shown in Figure 3A. The results of compound **7g** showed that the compound intersected within the second quadrant. The analysis confirmed that V_{\max} was reduced to new growing doses of inhibitor, on the other hand K_m stays the same. This behavior suggests that compound **7g** inhibits the alkaline phosphatase non-competitively to shape an enzyme-inhibitor complex. A secondary plot of slope against the concentrations of inhibitor confirmed enzyme-inhibitor dissociation constant (K_i) Figure 3B. The kinetic results are presented in Table 2.

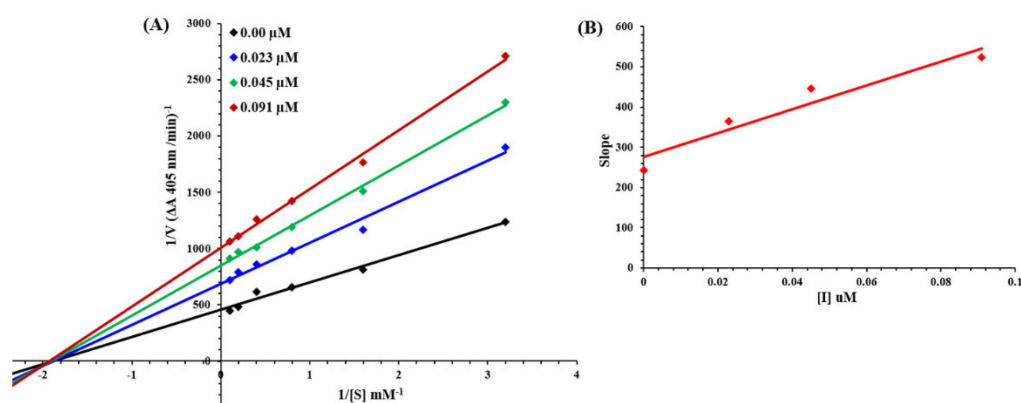


Figure 3. Lineweaver-Burk plots for the inhibition of alkaline phosphatase in the presence of compound **7g** (A). The insets represent the plot of the slope as opposed to inhibitor concentrations to determine the inhibition constant (B). The lines were drawn using linear least squares fit.

Table 2. Kinetic parameters of the compound **7g** for the alkaline phosphatase.

Concentrations (μM)	V_{max} ($\Delta\text{A}/\text{Min}$)	K_m (mM)	Inhibition Type	K_i (μM)
0.000	0.0023	0.5	Non-Competitive	0.093
0.023	0.0014	0.5		
0.045	0.0011	0.5		
0.091	0.0009	0.5		

V_{max} = the reaction velocity; K_m = Michaelis-Menten constant; K_i = EI dissociation constant.

2.2.3. Free Radical Scavenging Activity

All synthesized target compounds were assessed for 2, 2-diphenyl-1-picrylhydrazyl (DPPH) free radical scavenging ability. From our results, all of the compounds showed activity (Figure 4), but the most effective compound (**7g**) showed a bit of inhibition (29.7%) compared to the others at the concentration of 100 $\mu\text{g}/\text{mL}$. Ascorbic acid (vitamin C) was employed as a reference to evaluate the radical scavenging activity.

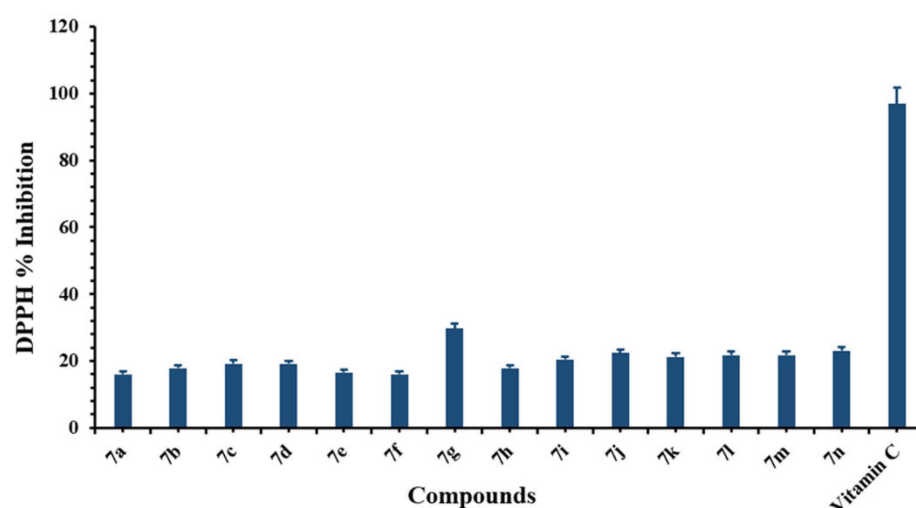


Figure 4. Free radical % scavenging activity of synthesized compounds (**7a–7n**). Values were depicted as mean \pm SEM.

2.2.4. Cell Viability

In this experiment, all fourteen pyrazolo-oxothiazolidine derivatives (**7a–7n**) after confirmation activity against in vitro ALP enzyme inhibition were carried out to check their toxic

effect on the human osteosarcoma MG-63 cell lines using the MTT assay technique. At first, four concentrations (0.5, 1, 2, and 4 μM) were chosen for each compound, along with a positive control (erlotinib), and all compounds and the standard drug were treated and incubated for 24 h. Normal control was considered to be 100% viable without any treatment. The viability of the cells was examined after incubation, and the results are presented in (Figure 5). From these results, it is clear that all compounds have no toxic effect on the cells, and even at the concentration of 4 μM , the cells were viable up to >70% except the compounds 7e, 7j, and 7m. However, at the first three treatments, all the compounds along with the standard drug showed >90% viability. These findings suggest that these compounds could be employed as a safe target for drug design within pharmaceutical approaches.

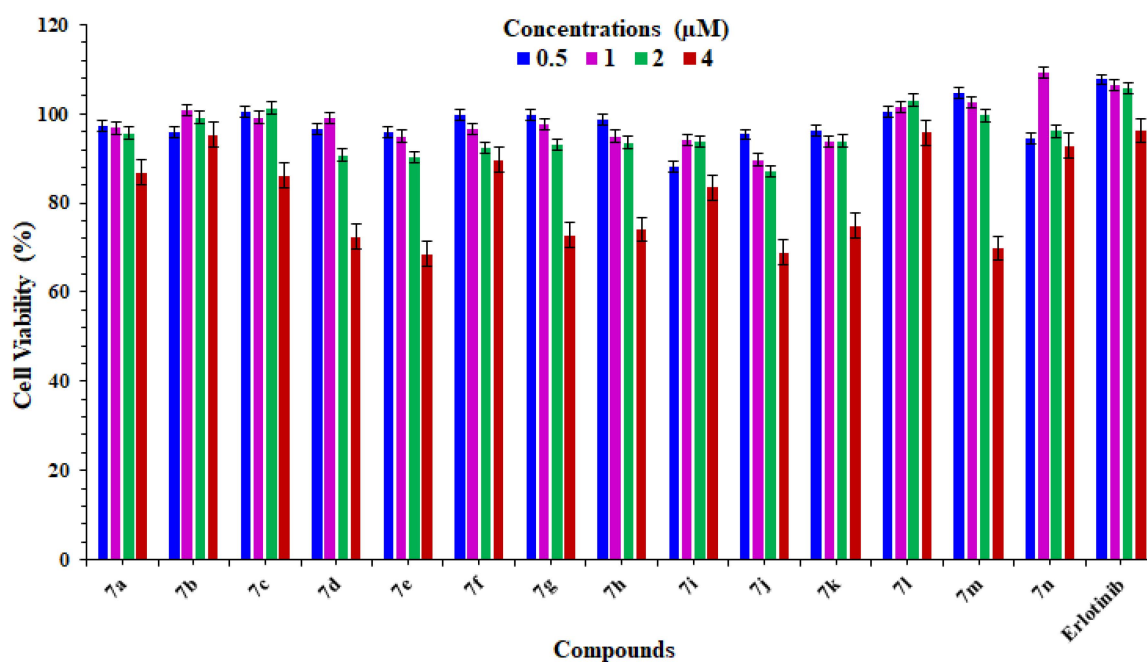


Figure 5. Cell viability results of synthesized compounds (7a–7n) on the human osteosarcoma MG-63 cell lines using the MTT assay at different concentrations for 24 h.

2.3. In Silico

2.3.1. Biochemical Properties and Lipinski's Rule of Five (RO5) Validation

The biochemical properties of all synthesized compounds (7a–7n) were predicted and analyzed through computational resources. The synthesized target compounds (7a–7n) were validated through RO5 analysis. The standard parameters in RO5 showed that the molecular mass and $\log P$ values must be less than 500 (g/mol) and 5, respectively. Moreover, the compounds should possess no greater than 10 HBA and 5 HBD, correspondingly. According to the literature, excessive values of HBA and HBD result in poor permeation [59,60]. The hydrogen-bonding capacity has been considered a significant parameter for drug permeability. Our results demonstrated the synthesized ligands possessed <10 HBA and <5 HBD values, which were comparable to standard values. However, the $\log P$ values in most compounds were also comparable with standard values (>5). The molecular weight (g/mol) of all compounds exceeded the standard value (Table 3). However, there are many examples available which deviate RO5 violation amongst the existing drugs [61,62]. Polar surface area (PSA) is also considered a good descriptor for characterizing drug absorption, including intestinal absorption, bioavailability, and blood–brain barrier penetration. Our predicted results showed that all compounds possess <140 \AA^2 values, which showed their good lead-like behavior. The drug-likeness score is a mixture of a complex balance of various molecular properties and structural features of chemical compounds, which determine whether the molecule is like as-known drugs [63]. Our results showed that all

the synthetic compounds (**7a–7n**) showed good drug score values. The majority of the compounds exhibited positive drug score values, whereas **7b** and **7n** possessed negative score values (Table 3).

Table 3. Biological properties of synthesized compounds.

Ligands	Mol. Weight (g/mol)	No. HBA	No. HBD	Mol. LogP	MolPSA (Å ²)	Mol. Vol (Å ³)	Drug Likeness Score
7a	483	6	0	5.46	56	430	0.09
7b	419	6	0	5.07	56	429	−0.01
7c	435	7	0	4.58	56	429	0.07
7d	541	8	0	5.83	71	545	0.02
7e	449	7	0	5.14	63	461	0.00
7f	503	7	0	6.14	63	475	0.58
7g	571	9	0	5.91	78	577	0.04
7h	513	7	0	5.54	63	462	0.14
7i	453	7	0	4.76	63	446	0.32
7j	435	7	0	4.70	63	440	0.07
7k	465	8	0	4.65	71	472	0.07
7l	439	6	0	5.22	56	426	0.44
7m	469	7	0	5.29	63	457	0.52
7n	405	6	0	4.62	56	408	−0.26

2.3.2. Structural Analysis and Physicochemical Properties of ALP

Human placental alkaline phosphatase is a class of hydrolase single-chain protein, having 539 amino acids with embedded zinc and magnesium ions at different structural sites. The VADAR analysis showed the overall protein architecture consists of 31% helices, 26% β sheets, and 42% coils. Moreover, the Ramachandran plot indicated that 96.4% of residues were present in favored regions which showed the precision of phi (ϕ) and psi (ψ) angles among the coordinates of ALP (Figure 6).

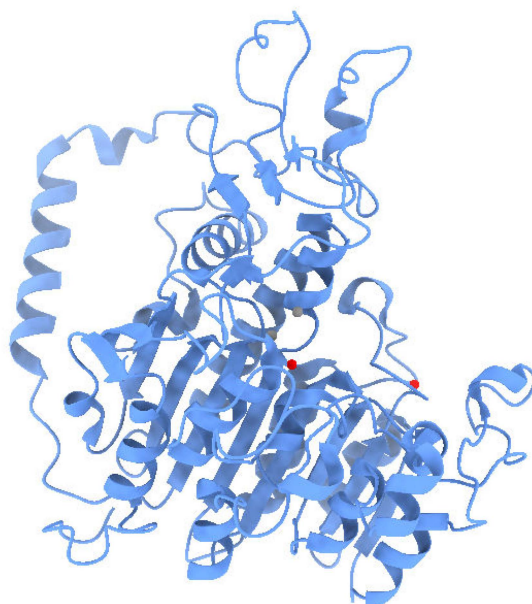


Figure 6. Three-dimensional structure of ALP.

2.3.3. Binding Energy Evaluation of Compounds

To predict the best conformational position within the active region of the target protein, all the synthesized ligands (**7a–7n**) were docked against ALP. All the generated docked complexes were analyzed based on minimum energy values (kcal/mol) and hydrogen/hydrophobic interactions. Docking results justified that all the synthesized target compounds exhibited good docking binding affinities with ALP. Both **7d** (−8.3 Kcal/mol) and **7g** (−8.1 Kcal/mol) exhibited higher binding energy values as compared to other

synthesized ligands. The remaining compounds showed different binding energy values, and most of the ligands were bound within the active region of the target protein. The basic chemical nuclei of all the synthesized compounds were the same; therefore, most ligands showed a good binding affinity with the target protein (Table 4).

Table 4. Docking energy values of synthesized ligands against ALP.

Docking Complexes	Docking Energy (Kcal/mol)
ALP_7a	−7.8
ALP_7b	−7.9
ALP_7c	−7.7
ALP_7d	−8.3
ALP_7e	−7.9
ALP_7f	−8
ALP_7g	−8.1
ALP_7h	−7.5
ALP_7i	−7.9
ALP_7j	−7.9
ALP_7k	−7.7
ALP_7l	−7.9
ALP_7m	−7.9
ALP_7n	−7.9

2.3.4. Binding Interaction of 7g against ALP

Based on in vitro (IC_{50}) results, the 7g-docked complex was selected to understand the binding interaction behavior of the compound against ALP. Docking analysis showed that 7g was actively confined within the active binding region of ALP (Figure 7). In detail, the SAR study showed that four hydrogen bonds were observed in the 7g-docking complex. The oxygen atom of 7g forms two hydrogen bonds with His₁₅₃ and His₃₁₇ having bond lengths 1.78 and 2.55 Å, respectively. The importance of these amino acid residues in binding with other ALP inhibitors has also been well documented [64,65]. The comparative binding energy and SAR analysis showed a significance of 7g and may be considered as a potent inhibitor of the enzyme. The rest of all docking complexes have been shown in Supplementary Data (Figures S43–S56).

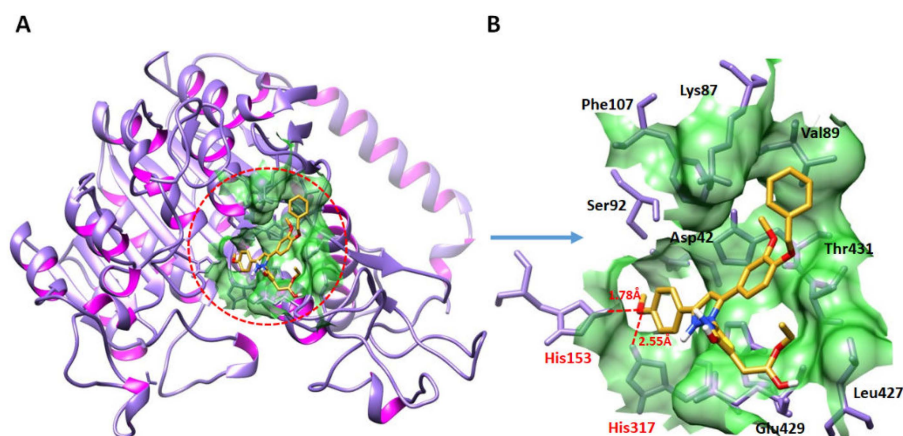


Figure 7. Docking complex of 7g against ALP (A,B).

3. Methods and Materials

3.1. Chemicals and Instruments

The MPA 160 apparatus of Fisher Scientific [Waltham, MA, USA] was used to determine the melting points (uncorrected) of the synthesized compounds. The FT-IR spectra was obtained using a Frontier IR spectrophotometer (Perkin Elmer, Waltham, MA, USA).

^1H NMR and ^{13}C NMR spectra of the compounds were recorded on a Bruker Avance III (Karlsruhe, Germany) at 400 and 100 MHz spectrophotometers using CDCl_3 as solvent. Chemical shifts were reported in parts per million (ppm) (δ). A thin layer chromatography (TLC) method was used to monitor the progress of the reaction. All commercially available chemicals and reagents were utilized without further purification.

3.2. General Procedure for the Synthesis of the Compounds

3.2.1. Procedure for Synthesis of Chalcones (3a–3n)

Acetophenone or 4-methoxyacetophenone (**1a** and **1b**, 1 mmol) was dissolved in approximately 10 mL of absolute ethyl alcohol and stirred for 5 min in an ice bath, as shown in Scheme 1. The sodium hydroxide (1.1 mmol) was then added portion-wise to the reaction flask. Following that, various substituted aromatic aldehydes (**2a–2h**, 1 mmol) were slowly added to the reaction mixture and stirred for 24 h in an ice bath. When the reaction was completed (determined by thin layer chromatography) the reaction mixture was poured into crushed ice and neutralized with hydrochloric acid. The obtained precipitate was stirred for 30 min at room temperature and then filtered, washed with cold water/ethanol, and dried to afford the desired chalcones (**3a–3n**) [66].

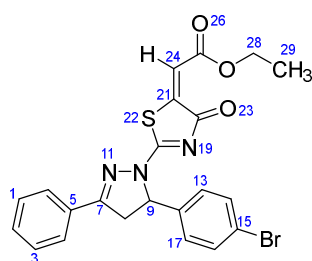
3.2.2. Procedure for Synthesis of 1-Thiocarbamoyl Pyrazole Derivatives (5a–5n)

As displayed in Scheme 1, 1.5 mmol thiosemicarbazide (**4**) and absolute ethanol were mixed for 10 min. Then, under the nitrogen atmosphere, 1.1 mmol potassium hydroxide was added and stirred for another 5–10 min, followed by the addition of corresponding chalcones (**3a–3n**, 1 mmol). The reaction was subsequently continued under reflux for 8 h until the reaction was completed (monitored by thin layer chromatography). The product was poured into crushed ice, neutralized with hydrochloric acid, stirred for 30 min, then filtered, washed with cold ethanol, and dried to obtain the 1-thiocarbamoyl pyrazole derivatives (**5a–5n**) [67].

3.2.3. Procedure for Synthesis of 1-Thiazolyl-2-Pyrazoline Derivatives (7a–7n)

As presented in Scheme 1, to a suspension of 1-thiocarbamoyl pyrazole compounds (**5a–5n**, 1 mmol) in absolute ethanol, diethyl acetylenedicarboxylate (**6**, 1 mmol) was added and followed by refluxing for 4 h. The reaction mixture was cooled at room temperature after completion (as confirmed by thin layer chromatography), and the precipitate was filtered and recrystallized from ethanol to achieve the desired target compounds (**7a–7n**) in good yields (80–92%).

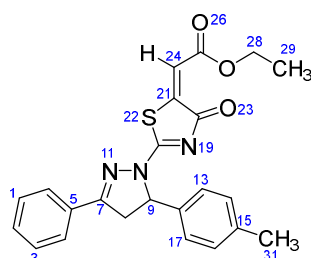
Ethyl-2-(2-(5-(4-bromophenyl)-3-phenyl-4,5-dihydro-1H-pyrazol-1-yl)-4-oxothiazol-5(4H)-ylidene)acetate (**7a**)



Yellow solid, isolated yield: 84%; mp: 242–244 °C. Figure S1: IR (KBr) ν (cm^{-1}): 2974 (C–H, alkane, stretching), 1694 (C=O, ester), 1602 (C=C, alkene), 1548, 1498 (C=C, aromatic), 1489 (C=N, stretching), 1218 (C–O, stretching), 1177, 1114, 1073, 1010 (C–N stretching and aromatic C–H out of plane bending), 823, 767, 757 (aromatic C–H out of plane bending), 689 (C–Br stretching). Figure S2: ^1H NMR (400 MHz, CDCl_3) δ (ppm): 1.37 (t, $J = 8$ Hz, 3H, CH_3 -29), 3.43 (dd, $J = 18, 4$ Hz, 1H, H-8_A), 4.03 (dd, $J = 18, 12$ Hz, 1H, H-8_B), 4.34 (q, $J = 7.2$ Hz, 2H, CH_2 -28), 5.85 (dd, $J = 11.2, 4$ Hz, 1H, H-9), 6.93 (s, 1H, H-24), 7.14–7.18 (m, 2H,

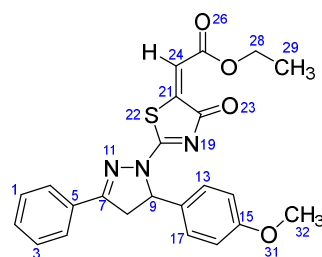
H-13 & 17), 7.46–7.58 (m, 5H, H-1, 2, 3, 4 & 6), 7.83–7.85 (m, 2H, H-14 & 16). Figure S3: ^{13}C NMR (100 MHz, CDCl_3) δ (ppm): 14.23 (C-29), 43.30 (C-8), 61.75 (C-28), 63.38 (C-9), 118.17 (C-24), 122.65 (C-15), 127.52 (C-4 & 6), 127.68 (C-13 & 17), 129.11 (C-1 & 3), 129.43 (C-2), 132.16 (C-5), 132.39 (C-14 & 16), 138.15 (C-12), 146.52 (C-21), 160.79 (C-7), 166.59 (C-25), 173.81 (C-20), 178.68 (C-18).

Ethyl-2-(4-oxo-2-(3-phenyl-5-(p-tolyl)-4,5-dihydro-1H-pyrazol-1-yl)thiazol-5(4H)-ylidene)acetate (**7b**)



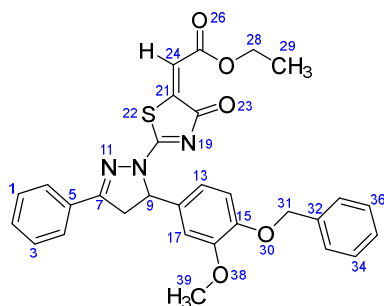
Yellow solid, isolated yield: 81%; mp: 226–228 °C. Figure S4: IR (KBr) ν (cm^{-1}): 2979 (C-H, alkane, stretching), 1694 (C=O, ester), 1602 (C=C, alkene), 1554, 1495 (C=C, aromatic), 1447 (C=N, stretching), 1225 (C-O, stretching), 1184, 1127, 1025 (C-N stretching and aromatic C-H out of plane bending), 833, 769, 757 (aromatic C-H out of plane bending). Figure S5: ^1H NMR (400 MHz, CDCl_3) δ (ppm): 1.37 (t, $J = 8$ Hz, 3H, CH_3 -29), 2.33 (s, 3H, CH_3 -31), 3.45 (dd, $J = 16, 4$ Hz, 1H, H-8_A), 4.00 (dd, $J = 18, 12$ Hz, 1H, H-8_B), 4.33 (q, $J = 8$ Hz, 2H, CH_2 -28), 5.86 (dd, $J = 12, 4$ Hz, 1H, H-9), 6.92 (s, 1H, H-24), 7.14–7.19 (m, 4H, H-13, 14, 16 & 17), 7.48–7.58 (m, 3H, H-1, 2 & 3), 7.85–7.87 (m, 2H, H-4 & 6). Figure S6: ^{13}C NMR (100 MHz, CDCl_3) δ (ppm): 14.24 (C-29), 21.16 (C-31), 43.46 (C-8), 61.67 (C-28), 63.85 (C-9), 117.79 (C-24), 125.86 (C-4 & 6), 127.51 (C-13 & 17), 129.05 (C-1 & 3), 129.68 (C-2), 129.85 (C-14 & 16), 131.99 (C-5), 136.25 (C-12), 138.48 (C-15), 146.81 (C-21), 161.02 (C-7), 166.66 (C-25), 173.59 (C-20), 178.81 (C-18).

Ethyl-2-(2-(5-(4-methoxyphenyl)-3-phenyl-4,5-dihydro-1H-pyrazol-1-yl)-4-oxothiazol-5(4H)-ylidene)acetate (**7c**)



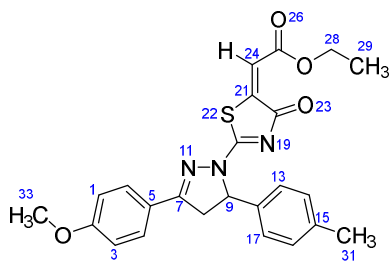
Yellow solid, isolated yield: 82%; mp: 236–238 °C. Figure S7: IR (KBr) ν (cm^{-1}): 2937 (C-H, alkane, stretching), 1693 (C=O, ester), 1601 (C=C, alkene), 1539, 1515 (C=C, aromatic), 1455 (C=N, stretching), 1243 (C-O, stretching), 1179, 1165, 1095, 1022 (C-N stretching and aromatic C-H out of plane bending), 827, 767, 720 (aromatic C-H out of plane bending). Figure S8: ^1H NMR (400 MHz, CDCl_3) δ (ppm): 1.37 (t, $J = 8$ Hz, 3H, CH_3 -29), 3.47 (dd, $J = 18, 4$ Hz, 1H, H-8_A), 3.80 (s, 3H, OCH_3 -32), 3.99 (dd, $J = 18, 12$ Hz, 1H, H-8_B), 4.33 (q, $J = 8$ Hz, 2H, CH_2 -28), 5.84 (dd, $J = 10, 4$ Hz, 1H, H-9), 6.85–6.89 (m, 2H, H-14 & 16), 6.92 (s, 1H, H-24), 7.21–7.25 (m, 2H, H-13 & 17), 7.49–7.58 (m, 3H, H-1, 2 & 3), 7.85–7.88 (m, 2H, H-4 & 6). Figure S9: ^{13}C NMR (100 MHz, CDCl_3) δ (ppm): 14.24 (C-29), 43.32 (C-8), 55.33 (C-32), 61.67 (C-28), 63.62 (C-9), 114.50 (C-14 & 16), 117.78 (C-24), 127.44 (C-4 & 6), 127.51 (C-13 & 17), 129.07 (C-1 & 3), 129.69 (C-2), 131.25 (C-12), 132.00 (C-5), 146.79 (C-21), 159.72 (C-7), 161.05 (C-15), 166.66 (C-25), 173.55 (C-20), 178.84 (C-18).

Ethyl-2-(2-(5-(4-(benzyloxy)-3-methoxyphenyl)-3-phenyl-4,5-dihydro-1H-pyrazol-1-yl)-4-oxothiazol-5(4H)-ylidene)acetate (7d)



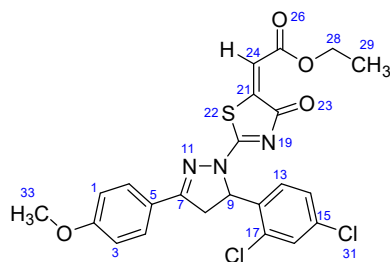
Yellow solid, isolated yield: 84%; mp: 202–204 °C. Figure S10: IR (KBr) ν (cm^{-1}): 2951 (C-H, alkane, stretching), 1703, 1686 (C=O, stretching), 1600 (C=C, alkene), 1540, 1497 (C=C, aromatic), 1448 (C=N, stretching), 1230 (C-O, stretching), 1189, 1166, 1134, 1115, 1024 (C-N stretching and aromatic C-H out of plane bending), 863, 762, 737 (aromatic C-H out of plane bending). Figure S11: ^1H NMR (400 MHz, CDCl_3) δ (ppm): 1.37 (t, $J = 8$ Hz, 3H, CH_3 -29), 3.46 (dd, $J = 16, 4$ Hz, 1H, H-8_A), 3.87 (s, 3H, OCH_3 -39), 3.97 (dd, $J = 16, 12$ Hz, 1H, H-8_B), 4.34 (q, $J = 8$ Hz, 2H, CH_2 -28), 5.13 (s, 2H, CH_2 -31), 5.84 (dd, $J = 10, 4$ Hz, 1H, H-9), 6.73 (dd, $J = 8.4, 2$ Hz, 1H, H-14), 6.81 (s, 1H, H-17), 6.83–6.84 (m, 1H, H-13), 6.93 (s, 1H, H-24), 7.30–7.43 (m, 5H, H-1, 3, 34, 35 & 36), 7.49–7.58 (m, 3H, H-2, 33 & 37), 7.85 (d, $J = 8$ Hz, 2H, H-4 & 6). Figure S12: ^{13}C NMR (100 MHz, CDCl_3) δ (ppm): 14.24 (C-29), 43.36 (C-8), 56.22 (C-39), 61.70 (C-28), 63.82 (C-9), 71.04 (C-31), 109.93 (C-17), 114.18 (C-14), 117.88 (C-24), 117.92 (C-13), 127.23 (C-4 & 6), 127.51 (C-33 & 37), 127.91 (C-35), 128.60 (C-34 & 36), 129.07 (C-1 & 3), 129.64 (C-2), 132.03 (C-12), 132.12 (C-5), 136.91 (C-32), 146.74 (C-21), 148.42 (C-15), 150.01 (C-16), 161.08 (C-7), 166.66 (C-25), 173.65 (C-20), 178.79 (C-18).

Ethyl-2-(2-(3-(4-methoxyphenyl)-5-(p-tolyl)-4,5-dihydro-1H-pyrazol-1-yl)-4-oxothiazol-5(4H)-ylidene)acetate (7e)



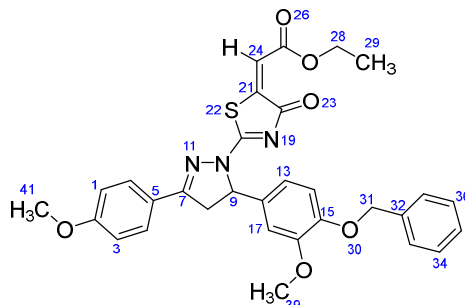
Yellow solid, isolated yield: 86%; mp: 208–210 °C. Figure S13: IR (KBr) ν (cm^{-1}): 2967 (C-H, alkane, stretching), 1687 (C=O, ester), 1607 (C=C, alkene), 1557, 1512 (C=C, aromatic), 1463 (C=N, stretching), 1250, 1226 (C-O, stretching), 1172, 1113, 1027 (C-N stretching and aromatic C-H out of plane bending), 830, 769, 720 (aromatic C-H out of plane bending). Figure S14: ^1H NMR (400 MHz, CDCl_3) δ (ppm): 1.37 (t, $J = 8$ Hz, 3H, CH_3 -29), 2.33 (s, 3H, CH_3 -31), 3.41 (dd, $J = 20, 4$ Hz, 1H, H-8_A), 3.91 (s, 3H, OCH_3 -33), 3.96 (dd, $J = 16, 12$ Hz, 1H, H-8_B), 4.33 (q, $J = 8$ Hz, 2H, CH_2 -28), 5.83 (dd, $J = 12, 4$ Hz, 1H, H-9), 6.91 (s, 1H, H-24), 6.98–7.02 (m, 2H, H-1 & 3), 7.14–7.18 (m, 4H, H-13, 14, 16 & 17), 7.78–7.82 (m, 2H, H-4 & 6). Figure S15: ^{13}C NMR (100 MHz, CDCl_3) δ (ppm): 14.23 (C-29), 21.15 (C-31), 43.46 (C-8), 55.55 (C-33), 61.62 (C-28), 63.76 (C-9), 114.47 (C-1 & 3), 117.52 (C-24), 122.23 (C-5), 125.86 (C-4 & 6), 129.34 (C-13 & 17), 129.81 (C-14 & 16), 136.34 (C-12), 138.41 (C-15), 147.01 (C-21), 160.74 (C-7), 162.68 (C-2), 166.72 (C-25), 172.97 (C-20), 178.77 (C-18).

Ethyl-2-(2-(5-(2,4-dichlorophenyl)-3-(4-methoxyphenyl)-4,5-dihydro-1H-pyrazol-1-yl)-4-oxothiazol-5(4H)-ylidene)acetate (**7f**)



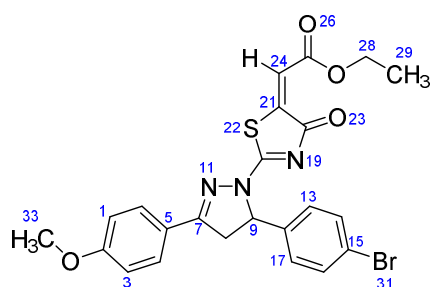
White solid, isolated yield: 90%; mp > 260 °C. Figure S16: IR (KBr) ν (cm^{-1}): 2974 (C-H, alkane, stretching), 1688 (C=O, ester), 1607 (C=C, alkene), 1591, 1547 (C=C, aromatic), 1513 (C=N, stretching), 1254, 1227 (C-O, stretching), 1177, 1119, 1099, 1028 (C-N stretching and aromatic C-H out of plane bending), 856 (C-Cl, stretching), 837, 770, 730 (aromatic C-H out of plane bending). Figure S17: ^1H NMR (400 MHz, CDCl_3) δ (ppm): 1.38 (t, $J = 8$ Hz, 3H, CH_3 -29), 3.29 (dd, $J = 18, 4$ Hz, 1H, H-8_A), 3.90 (s, 3H, OCH_3 -32), 4.07 (dd, $J = 20, 12$ Hz, 1H, H-8_B), 4.35 (q, $J = 8$ Hz, 2H, CH_2 -28), 6.11 (dd, $J = 12, 4$ Hz, 1H, H-9), 6.95–6.99 (m, 4H, H-1, 3, 13 & 24), 7.21 (dd, $J = 8.4, 1$ Hz, 1H, H-14), 7.47 (d, $J = 2$ Hz, 1H, H-16), 7.75–7.79 (m, 2H, H-4 & 6). Figure S18: ^{13}C NMR (100 MHz, CDCl_3) δ (ppm): 14.24 (C-29), 42.61 (C-8), 55.56 (C-33), 61.47 (C-28), 61.77 (C-9), 114.49 (C-1 & 3), 118.23 (C-24), 121.85 (C-13), 127.03 (C-14), 127.82 (C-5), 129.35 (C-4 & 6), 130.22 (C-17), 132.47 (C-15), 134.82 (C-12), 134.87 (C-16), 146.63 (C-21), 160.61 (C-7), 162.82 (C-2), 166.64 (C-25), 173.49 (C-20), 178.64 (C-18).

Ethyl-2-(2-(5-(4-(benzyloxy)-3-methoxyphenyl)-3-(4-methoxyphenyl)-4,5-dihydro-1H-pyrazol-1-yl)-4-oxothiazol-5(4H)-ylidene)acetate (**7g**)



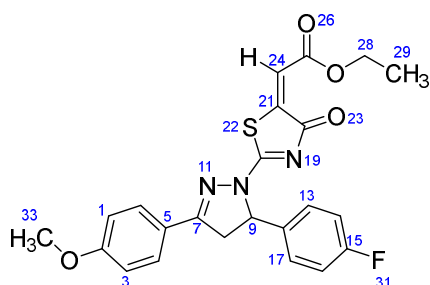
Yellow solid, isolated yield: 85%; mp: 228–230 °C. Figure S19: IR (KBr) ν (cm^{-1}): 2996, 2948 (C-H, alkane, stretching), 1703, 1684 (C=O, stretching), 1610 (C=C, alkene), 1597, 1549 (C=C, aromatic), 1514 (C=N, stretching), 1262, 1228 (C-O, stretching), 1192, 1174, 1135, 1117, 1016 (C-N stretching and aromatic C-H out of plane bending), 864, 834, 746, 724 (aromatic C-H out of plane bending). Figure S20: ^1H NMR (400 MHz, CDCl_3) δ (ppm): 1.37 (t, $J = 8$ Hz, 3H, CH_3 -29), 3.41 (dd, $J = 18, 4$ Hz, 1H, H-8_A), 3.87 (s, 3H, OCH_3 -39), 3.90 (s, 3H, OCH_3 -41), 3.94 (dd, $J = 18, 12$ Hz, 1H, H-8_B), 4.33 (q, $J = 8$ Hz, 2H, CH_2 -28), 5.13 (s, 2H, CH_2 -31), 5.81 (dd, $J = 12, 4$ Hz, 1H, H-9), 6.73 (dd, $J = 8, 4$ Hz, 1H, H-14), 6.80 (s, 1H, H-17), 6.83–6.84 (m, 1H, H-13), 6.92 (s, 1H, H-24), 6.98–7.01 (m, 2H, H-1 & 3), 7.30–7.43 (m, 5H, H-33, 34, 35, 36 & 37), 7.77–7.81 (m, 2H, H-4 & 6). Figure S21: ^{13}C NMR (100 MHz, CDCl_3) δ (ppm): 14.24 (C-29), 43.35 (C-8), 55.55 (C-41), 56.21 (C-39), 61.64 (C-28), 63.73 (C-9), 71.05 (C-31), 109.95 (C-17), 114.17 (C-14), 114.48 (C-1 & 3), 117.59 (C-24), 117.94 (C-13), 122.18 (C-5), 127.23 (C-4 & 6), 127.89 (C-35), 128.59 (C-33 & 37), 129.34 (C-34 & 36), 132.24 (C-12), 136.94 (C-32), 146.95 (C-21), 148.38 (C-15), 149.99 (C-16), 160.81 (C-7), 162.71 (C-2), 166.71 (C-25), 173.01 (C-20), 178.76 (C-18).

Ethyl-2-(2-(5-(4-bromophenyl)-3-(4-methoxyphenyl)-4,5-dihydro-1H-pyrazol-1-yl)-4-oxothiazol-5(4H)-ylidene)acetate (**7h**)



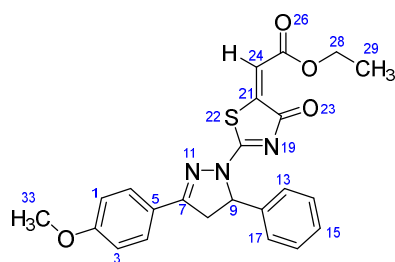
Yellow solid, isolated yield: 89%; mp: 218–220 °C. Figure S22: IR (KBr) ν (cm^{-1}): 2969 (C-H, alkane, stretching), 1687 (C=O, ester), 1607 (C=C, alkene), 1588, 1542 (C=C, aromatic), 1511, 1488 (C=N, stretching), 1308, 1249 (C-O, stretching), 1177, 1105, 1030, 1008 (C-N stretching and aromatic C-H out of plane bending), 844, 836, 814, 768, 724 (aromatic C-H out of plane bending), 658 (C-Br stretching). Figure S23: ^1H NMR (400 MHz, CDCl_3) δ (ppm): 1.37 (t, $J = 8$ Hz, 3H, CH_3 -29), 3.39 (dd, $J = 16$, 4 Hz, 1H, H-8_A), 3.91 (s, 3H, OCH_3 -33), 3.99 (dd, $J = 18$, 12 Hz, 1H, H-8_B), 4.34 (q, $J = 8$ Hz, 2H, CH_2 -28), 5.82 (dd, $J = 10$, 4 Hz, 1H, H-9), 6.92 (s, 1H, H-24), 6.99–7.02 (m, 2H, H-1 & 3), 7.15–7.18 (m, 2H, H-13 & 17), 7.46–7.50 (m, 2H, H-14 & 16), 7.77–7.80 (m, 2H, H-4 & 6). Figure S24: ^{13}C NMR (100 MHz, CDCl_3) δ (ppm): 14.23 (C-29), 43.29 (C-8), 55.57 (C-33), 61.70 (C-28), 63.29 (C-9), 114.53 (C-1 & 3), 117.89 (C-24), 121.96 (C-15), 122.59 (C-5), 127.69 (C-4 & 6), 129.37 (C-13 & 17), 132.36 (C-14 & 16), 138.25 (C-12), 146.72 (C-21), 160.48 (C-7), 162.81 (C-2), 166.65 (C-25), 173.20 (C-20), 178.66 (C-18).

Ethyl-2-(2-(5-(4-fluorophenyl)-3-(4-methoxyphenyl)-4,5-dihydro-1H-pyrazol-1-yl)-4-oxothiazol-5(4H)-ylidene)acetate (**7i**)



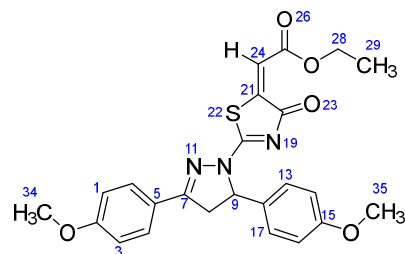
Yellow solid, isolated yield: 88%; mp: 210–212 °C. Figure S25: IR (KBr) ν (cm^{-1}): 2975 (C-H, alkane, stretching), 1686 (C=O, ester), 1604 (C=C, alkene), 1544, 1510 (C=C, aromatic), 1474 (C=N, stretching), 1311, 1222 (C-O, stretching), 1184 (C-F, stretching), 1174, 1111, 1039 (C-N stretching and aromatic C-H out of plane bending), 858, 831, 809, 769, 729 (aromatic C-H out of plane bending). Figure S26: ^1H NMR (400 MHz, CDCl_3) δ (ppm): 1.37 (t, $J = 8$ Hz, 3H, CH_3 -29), 3.40 (dd, $J = 16$, 4 Hz, 1H, H-8_A), 3.91 (s, 3H, OCH_3 -33), 3.98 (dd, $J = 16$, 12 Hz, 1H, H-8_B), 4.33 (q, $J = 8$ Hz, 2H, CH_2 -28), 5.85 (dd, $J = 12$, 4 Hz, 1H, H-9), 6.92 (s, 1H, H-24), 6.99–7.06 (m, 4H, H-1, 3, 14 & 16), 7.25–7.27 (m, 2H, H-13 & 17), 7.78–7.82 (m, 2H, H-4 & 6). Figure S27: ^{13}C NMR (100 MHz, CDCl_3) δ (ppm): 14.23 (C-29), 43.39 (C-8), 55.57 (C-33), 61.68 (C-28), 63.21 (C-9), 114.52 (C-1 & 3), 116.16 (d, $J = 21$ Hz, C-14 & 16), 117.79 (C-24), 122.03 (C-5), 127.87 (d, $J = 8.8$ Hz, C-13 & 17), 129.36 (C-4 & 6), 135.09 (d, $J = 3$ Hz, C-12), 146.77 (C-21), 160.57 (C-7), 162.62 (d, $J = 246$ Hz, C-15), 162.78 (C-2), 166.66 (C-25), 173.14 (C-20), 178.71 (C-18).

Ethyl-2-(2-(3-(4-methoxyphenyl)-5-phenyl-4,5-dihydro-1H-pyrazol-1-yl)-4-oxothiazol-5(4H)-ylidene)acetate (7j)



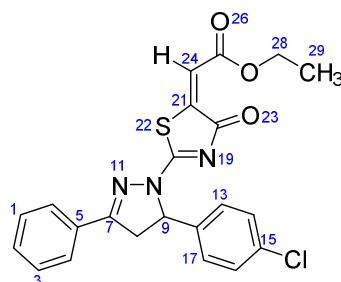
Yellow solid, isolated yield: 81%; mp: 167–169 °C. Figure S28: IR (KBr) ν (cm^{-1}): 2976 (C-H, alkane, stretching), 1686 (C=O, ester), 1606 (C=C, alkene), 1592, 1552 (C=C, aromatic), 1511, 1464 (C=N, stretching), 1309, 1249 (C-O, stretching), 1176, 1114, 1026 (C-N stretching and aromatic C-H out of plane bending), 858, 834, 768, 722 (aromatic C-H out of plane bending). Figure S29: ^1H NMR (400 MHz, CDCl_3) δ (ppm): 1.37 (t, $J = 8$ Hz, 3H, CH_3 -29), 3.42 (dd, $J = 20, 4$ Hz, 1H, H-8_A), 3.90 (s, 3H, OCH_3 -33), 3.98 (dd, $J = 18, 12$ Hz, 1H, H-8_B), 4.33 (q, $J = 8$ Hz, 2H, CH_2 -28), 5.87 (dd, $J = 12, 4$ Hz, 1H, H-9), 6.91 (s, 1H, H-24), 6.98–7.01 (m, 2H, H-1 & 3), 7.26–7.28 (m, 2H, H-14 & 16), 7.31–7.37 (m, 3H, H-13, 17 & 15), 7.78–7.81 (m, 2H, H-4 & 6). Figure S30: ^{13}C NMR (100 MHz, CDCl_3) δ (ppm): 14.24 (C-29), 43.49 (C-8), 55.56 (C-33), 61.64 (C-28), 63.90 (C-9), 114.48 (C-1 & 3), 117.62 (C-24), 122.15 (C-5), 125.83 (C-4 & 6), 128.53 (C-15), 129.19 (C-13 & 17), 129.36 (C-14 & 16), 139.26 (C-12), 146.94 (C-21), 160.71 (C-7), 162.71 (C-2), 166.69 (C-25), 173.07 (C-20), 178.76 (C-18).

Ethyl-2-(2-(3,5-bis(4-methoxyphenyl)-4,5-dihydro-1H-pyrazol-1-yl)-4-oxothiazol-5(4H)-ylidene)acetate (7k)



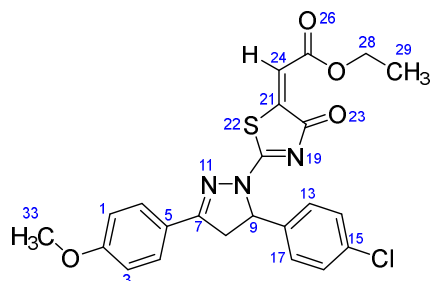
Yellow solid, isolated yield: 86%; mp: 208–210 °C. Figure S31: IR (KBr) ν (cm^{-1}): 2937, 2835 (C-H, alkane, stretching), 1693 (C=O, ester), 1609 (C=C, alkene), 1594, 1553 (C=C, aromatic), 1512, 1464 (C=N, stretching), 1311, 1248, 1222 (C-O, stretching), 1174, 1111, 1025 (C-N stretching and aromatic C-H out of plane bending), 862, 839, 809, 768, 728 (aromatic C-H out of plane bending). Figure S32: ^1H NMR (400 MHz, CDCl_3) δ (ppm): 1.36 (t, $J = 8$ Hz, 3H, CH_3 -29), 3.42 (dd, $J = 20, 4$ Hz, 1H, H-8_A), 3.79 (s, 3H, OCH_3 -34), 3.91 (s, 3H, OCH_3 -35), 3.96 (m, 1H, H-8_B), 4.33 (q, $J = 8$ Hz, 2H, CH_2 -28), 5.81 (dd, $J = 12, 4$ Hz, 1H, H-9), 6.84–6.87 (m, 2H, H-14 & 16), 6.90 (s, 1H, H-24), 6.98–7.02 (m, 2H, H-1 & 3), 7.20–7.24 (m, 2H, H-13 & 17), 7.78–7.82 (m, 2H, H-4 & 6). Figure S33: ^{13}C NMR (100 MHz, CDCl_3) δ (ppm): 14.24 (C-29), 43.33 (C-8), 55.32 (C-35), 55.56 (C-34), 61.62 (C-28), 63.53 (C-9), 114.46 (C-1, 3, 14 & 16), 117.48 (C-24), 122.22 (C-5), 127.44 (C-4 & 6), 129.35 (C-13 & 17), 131.35 (C-12), 146.98 (C-21), 159.66 (C-7), 160.82 (C-15), 162.69 (C-2), 166.71 (C-25), 172.91 (C-20), 178.81 (C-18).

Ethyl-2-(2-(5-(4-chlorophenyl)-3-phenyl-4,5-dihydro-1H-pyrazol-1-yl)-4-oxothiazol-5(4H)-ylidene)acetate (**7l**)

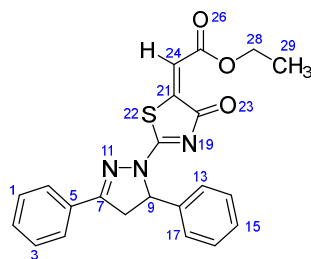


Yellow solid, isolated yield: 82%; mp: 251–253 °C. Figure S34: IR (KBr) ν (cm^{-1}): 2987, 2936 (C-H, alkane, stretching), 1684 (C=O, ester), 1601 (C=C, alkene), 1549, 1495 (C=C, aromatic), 1447 (C=N, stretching), 1227 (C-O, stretching), 1179, 1110, 1094, 1021 (C-N stretching and aromatic C-H out of plane bending), 862 (C-Cl, stretching), 829, 765, 727 (aromatic C-H out of plane bending). Figure S35: ^1H NMR (400 MHz, CDCl_3) δ (ppm): 1.37 (t, $J = 8$ Hz, 3H, CH_3 -29), 3.43 (dd, $J = 20, 4$ Hz, 1H, H-8_A), 4.03 (dd, $J = 18, 12$ Hz, 1H, H-8_B), 4.34 (q, $J = 8$ Hz, 2H, CH_2 -28), 5.87 (dd, $J = 12, 4$ Hz, 1H, H-9), 6.93 (s, 1H, H-24), 7.21–7.24 (m, 2H, H-1 & 3), 7.31–7.35 (m, 2H, H-13 & 17), 7.49–7.59 (m, 3H, H-14, 16 & 2), 7.84–7.86 (m, 2H, H-4 & 6). Figure S36: ^{13}C NMR (100 MHz, CDCl_3) δ (ppm): 14.23 (C-29), 43.35 (C-8), 61.75 (C-28), 63.33 (C-9), 118.16 (C-24), 127.39 (C-4 & 6), 127.52 (C-1 & 3), 129.11 (C-14 & 16), 129.44 (C-2, 13 & 17), 132.15 (C-5), 134.53 (C-15), 137.63 (C-12), 146.52 (C-21), 160.80 (C-7), 166.59 (C-25), 173.81 (C-20), 178.69 (C-18).

Ethyl-2-(2-(5-(4-chlorophenyl)-3-(4-methoxyphenyl)-4,5-dihydro-1H-pyrazol-1-yl)-4-oxothiazol-5(4H)-ylidene)acetate (**7m**)



Yellow solid, isolated yield: 92%; mp: 220–222 °C. Figure S37: IR (KBr) ν (cm^{-1}): 2971 (C-H, alkane, stretching), 1688 (C=O, ester), 1607 (C=C, alkene), 1589, 1542 (C=C, aromatic), 1513, 1493 (C=N, stretching), 1248 (C-O, stretching), 1177, 1106, 1087, 1031 (C-N stretching and aromatic C-H out of plane bending), 865 (C-Cl, stretching), 844, 814, 795, 768 (aromatic C-H out of plane bending). Figure S38: ^1H NMR (400 MHz, CDCl_3) δ (ppm): 1.37 (t, $J = 8$ Hz, 3H, CH_3 -29), 3.38 (dd, $J = 16, 4$ Hz, 1H, H-8_A), 3.91 (s, 3H, OCH_3 -33), 3.99 (dd, $J = 18, 12$ Hz, 1H, H-8_B), 4.33 (q, $J = 8$ Hz, 2H, CH_2 -28), 5.84 (dd, $J = 8, 4$ Hz, 1H, H-9), 6.91 (s, 1H, H-24), 6.98–7.02 (m, 2H, H-1 & 3), 7.20–7.23 (m, 2H, H-13 & 17), 7.30–7.33 (m, 2H, H-14 & 16), 7.77–7.81 (m, 2H, H-4 & 6). Figure S39: ^{13}C NMR (100 MHz, CDCl_3) δ (ppm): 14.23 (C-29), 43.34 (C-8), 55.57 (C-33), 61.69 (C-28), 63.24 (C-9), 114.52 (C-1 & 3), 117.85 (C-24), 121.97 (C-5), 127.40 (C-4 & 6), 129.37 (C-14 & 16), 129.39 (C-13 & 17), 134.44 (C-15), 137.74 (C-12), 146.72 (C-21), 160.54 (C-7), 162.80 (C-2), 166.64 (C-25), 173.17 (C-20), 178.66 (C-18).

Ethyl-2-(2-(3,5-diphenyl-4,5-dihydro-1H-pyrazol-1-yl)-4-oxothiazol-5(4H)-ylidene)acetate (**7n**)

Yellow solid, isolated yield: 80%; mp: 216–218 °C. Figure S40: IR (KBr) ν (cm^{-1}): 2985, 2928 (C-H, alkane, stretching), 1693 (C=O, ester), 1602 (C=C, alkene), 1540, 1495 (C=C, aromatic), 1455 (C=N, stretching), 1223 (C-O, stretching), 1185, 1170, 1112, 1033 (C-N stretching and aromatic C-H out of plane bending), 858, 825, 765, 742 (aromatic C-H out of plane bending). Figure S41: ^1H NMR (400 MHz, CDCl_3) δ (ppm): 1.37 (t, $J = 8$ Hz, 3H, CH_3 -29), 3.46 (dd, $J = 16$, 4 Hz, 1H, H-8_A), 4.02 (dd, $J = 16$, 12 Hz, 1H, H-8_B), 4.34 (q, $J = 8$ Hz, 2H, CH_2 -28), 5.90 (dd, $J = 12$, 4 Hz, 1H, H-9), 6.93 (s, 1H, H-24), 7.28–7.38 (m, 5H, H-13, 14, 15, 16 & 17), 7.48–7.58 (m, 3H, H-1, 2 & 3), 7.85–7.87 (m, 2H, H-4 & 6). Figure S42: ^{13}C NMR (100 MHz, CDCl_3) δ (ppm): 14.23 (C-29), 43.51 (C-8), 61.70 (C-28), 63.99 (C-9), 117.94 (C-24), 125.82 (C-4 & 6), 127.53 (C-13 & 17), 128.60 (C-15), 129.06 (C-1 & 3), 129.24 (C-14 & 16), 129.62 (C-2), 132.04 (C-5), 139.14 (C-12), 146.72 (C-21), 161.00 (C-7), 166.63 (C-25), 173.71 (C-20), 178.79 (C-18).

3.3. Biology

3.3.1. Alkaline Phosphatase Inhibition Assay

As previously mentioned [65,68], spectrophotometric analysis was used to evaluate the activity of calf intestinal alkaline phosphatase (CIAP). The reaction mixture contained 50 mM Tris-HCl buffer (5 mM MgCl_2 , 0.1 mM ZnCl_2 pH 9.5), the 10 μL compound, and it was preincubated for 10 min by adding 5 μL of CIAP (0.025 U/mL). Then, 10 μL of a substrate (0.5 mM *p*-NPP (para nitrophenyl phosphate disodium salt)) was delivered to initiate the response, and therefore the assay mixture became incubated once more for 30 min at 37 °C. The change in absorbance of released *p*-nitrophenolate was monitored at 405 nm, using a 96-well microplate reader (Thermo Scientific Multiskan GO, USA). All the experiments were repeated three times in a triplicate manner. KH_2PO_4 (potassium dihydrogen phosphate) was used as the reference inhibitor of CIAP. The inhibition activity was calculated according to the following equation:

$$\text{Inhibition (\%)} = [(Blank - Sample) / Blank] \times 100$$

For calculation of the IC_{50} values, 6–8 serial dilutions were used and the results examined using the non-linear regression analysis of GraphPad Prism 5 [69].

3.3.2. Kinetic Mechanism Analysis

Primarily based on the IC_{50} findings, we selected the most effective inhibitor **7g** for CIAP to determine the mechanism of enzyme inhibition using our published method [70]. The inhibitor (**7g**), and substrate *p*-NPP concentrations were used at 0.00, 0.023, 0.045 and 0.091 μM , 10, 5, 2.5, 1.25, 0.625 and 0.3125 mM, respectively. The pre-incubation time and other conditions were the same as those mentioned in the section on the CIAP assay. Maximal initial velocities were determined from the initial linear portion of absorbances up to 10 min after the addition of enzyme per minute interval. The inhibition type of the enzyme was assayed by the Lineweaver–Burk plot of inverse velocities ($1/V$) versus the inverse of substrate concentration $1/[S]$ mM^{-1} . The EI dissociation constant K_i was determined by a secondary plot of $1/V$ versus inhibitor concentration.

3.3.3. Free Radical Scavenging Assay

Free radical scavenging activity was determined by modifying the method by DPPH assay [71]. The assay solution composed of the 100 μ L of DPPH (150 μ M) and 20 μ L of the sample (100 μ g/mL) was introduced to gain the final volume of each well up to 200 μ L with methyl alcohol. Then, it was incubated in the dark at room temperature for the following half-hour. Ascorbic acid (Vitamin C) was used as a reference inhibitor. The measurements were performed by using a microplate reader (Thermo Scientific Multiskan GO, USA) at 517 nm. Each experiment was carried out in triplicate.

3.3.4. Cell Culture and Treatment of Compounds

The human osteosarcoma MG-63 cells were acquired from the Korean Cell Line Bank (Seoul, Korea). The MG-63 cell lines were incubated in the humidified atmosphere at 37 °C containing 5% CO₂ and maintained in the DMEM (Sigma, St. Louis, MO, USA), supplemented with 10% fetal bovine serum (FBS, WELGENE, Korea) and 50 unit/mL penicillin (Sigma) and 50 μ g/mL streptomycin (Sigma). The medium was completely renewed every two days. The synthesized compounds were completely dissolved in dimethyl sulfoxide (DMSO) and further diluted to various concentrations (0, 0.5, 1, 2, and 4 μ M). The control groups were treated with the same amount of DMSO.

3.3.5. Cell Viability

MTT assay technique was applied to check the toxic effect of our compounds. The MG-63 cell lines were seeded onto 96-well plates at a density of 0.4×10^5 cells/well with the medium for 24 h. After reaching 50% density, the cells were exposed to synthesized target compounds at the dose of 0, 0.5, 1, 2, and 4 μ M for 24 h in media. We employed erlotinib as a positive control to compare the results of the synthesized derivatives. After 24 h, the cell sustained 100 μ L DMEM containing of 0.5 mg/mL 3-(4,5-dimethylthiazol-2-yl)-2,5-diphenyltetrazolium bromide (MTT) at 37 °C for 4 h. Then, the purple formazan crystals were dissolved with 100 μ L of buffer (10% SDS, 0.01 N HCl). Finally, the absorbance was measured at 570 nm using a microplate reader (Thermo Fisher, Waltham, MA, USA).

3.4. Computational Methodology

3.4.1. Chemoinformatic Analysis of Designed Ligands

The synthesized ligands (7a–7n) were sketched in ACD/ChemSketch and further minimized by UCSF Chimera 1.10.1., whereas biochemical properties and Lipinski's rule of five (RO5) of synthesized compounds were predicted and justified, respectively, using online computational tools such as Molinspiration (<http://www.molinspiration.com/>) and Molsoft (<http://www.molsoft.com/> accessed on the 8 September 2022).

3.4.2. Retrieval of Alkaline Phosphate Structure from PDB

The three-dimensional (3D) structure of alkaline phosphate from the human placenta was accessed from Protein Data Bank (PDB) (www.rcsb.org) having PDBID 1EW2. The selected target protein structure was minimized by using the UCSF Chimera 1.10.1 tool [72,73]. The protein architecture and statistical percentage values of receptor proteins helices, β -sheets, coils, and turn were predicted from the online server VADAR 1.8 [74].

3.4.3. Designing of Ligands and Molecular Docking

The synthesized ligands were sketched in the drawing ACD/Chem Sketch tool and minimized by UCSF Chimera 1.10.1. All the synthesized ligands were sketched in ACD/Chem Sketch tool and accessed in mol format. Furthermore, the UCSF Chimera 1.10.1 tool was employed for energy minimization of each ligand separately having default parameters such as steepest descent steps 100 with step size 0.02 (Å), conjugate gradient steps 100 with step size 0.02 (Å), and update interval was fixed at 10. Finally, Gasteiger charges were added using Dock Prep in ligand structure to obtain the good structure conformation. The molecular docking experiment was used on all the synthesized ligands

against ALP by using the PyRx 0.8, virtual screening tool with Auto Dock VINA Wizard v.1.2.0. approach [75]. The grid box center values of (center X = 43.3, center Y = 23.1612, and center Z = 9.1269), and size values were adjusted as (X = 65.56, Y = 71.79, and Z = 64.64) for better conformational position in the active region of the target protein. All the synthesized ligands were docked separately against ALP with a default exhaustiveness value = 8. The predicted docked complexes were evaluated based on the lowest binding energy (kcal/mol) values and structure activity relationship (SAR). The three-dimensional graphical depictions of all the docked complexes were accomplished by Discovery Studio (2.1.0) and UCSF Chimera 1.10.1 tool.

4. Conclusions

In the current study, we have successfully synthesized and characterized fourteen pyrazolo-oxothiazolidine derivatives using a multistep synthetic process. All the synthesized compounds were evaluated for in vitro alkaline phosphatase inhibitor activity and found to be stronger than monopotassium phosphate. Among them, compound **7g** ($IC_{50} = 0.045 \pm 0.004 \mu M$) had the most effective inhibitory effect against alkaline phosphatases compared to the standard reference KH_2PO_4 ($IC_{50} = 5.242 \pm 0.472 \mu M$). Furthermore, the MTT assay was performed against MG-63 at various concentrations to screen the cell viability potential of synthesized compounds, and they showed no toxic effect on the viability of cells. Molecular docking studies were conducted, to determine the binding affinity of the ligands with the target protein within the active site, and all compounds exhibited good docking binding affinity with alkaline phosphatase and showed good docking scores. According to research findings, these compounds, particularly **7g**, might employ as worthwhile therapeutic candidates for alkaline phosphatase-associated disorders in medicinal chemistry.

Supplementary Materials: The following supporting information can be downloaded at: <https://www.mdpi.com/article/10.3390/ijms232113262/s1>. Reference [76] are cited in the Supplementary Materials.

Author Contributions: N.H.N. designed, synthesized, analyzed the data, and wrote the manuscript. H.R. performed the in vitro analysis. R.S.S. carried out the cytotoxicity experiments. M.H. and A.K. conducted the computational part. S.J.K. supervised and administrated the project. All authors contributed to the clarification of the manuscript's draft. All authors have read and agreed to the published version of the manuscript.

Funding: This work was supported by the National Research Foundation of Korea (NRF) funded by the Korean Government (MEST) (2020R1I1A306969913).

Institutional Review Board Statement: Not applicable.

Informed Consent Statement: Not applicable.

Data Availability Statement: The dataset generated during the current study will be available from the corresponding author upon reasonable request.

Acknowledgments: This work was supported by the National Research Foundation of Korea (NRF) funded by the Korean Government (MEST) (2020R1I1A306969913). MH acknowledges The Ohio State University for providing the "President's Postdoctoral Scholars Program (PPSP)" award for financial support to complete this computational research.

Conflicts of Interest: The authors have no conflicts of interest to declare that are relevant to the content of this article.

References

1. Chang, T.-C.; Wang, J.-K.; Hung, M.-W.; Chiao, C.-H.; Tsai, L.-C.; Chang, G.G. Regulation of the Expression of Alkaline Phosphatase in a Human Breast-Cancer Cell Line. *Biochem. J.* **1994**, *303*, 199–205. [[CrossRef](#)] [[PubMed](#)]
2. Whyte, M.P.; Landt, M.; Ryan, L.M.; Mulivor, R.A.; Henthorn, P.S.; Fedde, K.N.; Mahuren, J.D.; Coburn, S.P. Alkaline Phosphatase: Placental and Tissue-Nonspecific Isoenzymes Hydrolyze Phosphoethanolamine, Inorganic Pyrophosphate, and Pyridoxal 5'-Phosphate. Substrate Accumulation in Carriers of Hypophosphatasia Corrects during Pregnancy. *J. Clin. Invest.* **1995**, *95*, 1440–1445. [[CrossRef](#)] [[PubMed](#)]

3. McComb, R.B.; Bowers, G.N.; Posen, S. *Alkaline Phosphatase*; Springer: New York, NY, USA, 1979.
4. Tsai, L.; Hung, M.; Chen, Y.; Su, W.; Chang, G.; Chang, T. Expression and Regulation of Alkaline Phosphatases in Human Breast Cancer MCF-7 Cells. *Eur. J. Biochem.* **2000**, *267*, 1330–1339. [[CrossRef](#)] [[PubMed](#)]
5. Weiss, M.J.; Henthorn, P.S.; Lafferty, M.A.; Slaughter, C.; Raducha, M.; Harris, H. Isolation and Characterization of a cDNA Encoding a Human Liver/Bone/Kidney-Type Alkaline Phosphatase. *Proc. Natl. Acad. Sci. USA* **1986**, *83*, 7182–7186. [[CrossRef](#)] [[PubMed](#)]
6. Sharma, U.; Singh, S.K.; Pal, D.; Khajuria, R.; Mandal, A.K.; Prasad, R. Implication of BBM Lipid Composition and Fluidity in Mitigated Alkaline Phosphatase Activity in Renal Cell Carcinoma. *Mol. Cell. Biochem.* **2012**, *369*, 287–293. [[CrossRef](#)]
7. Benham, F.; Cottell, D.C.; Franks, L.M.; Wilson, P.D. Alkaline Phosphatase Activity in Human Bladder Tumor Cell Lines. *J. Histochem. Cytochem.* **1977**, *25*, 266–274. [[CrossRef](#)]
8. Mornet, E.; Stura, E.; Lia-Baldini, A.-S.; Stigbrand, T.; Ménez, A.; Le Du, M.-H. Structural Evidence for a Functional Role of Human Tissue Nonspecific Alkaline Phosphatase in Bone Mineralization. *J. Biol. Chem.* **2001**, *276*, 31171–31178. [[CrossRef](#)]
9. Millán, J.L. Alkaline Phosphatases. *Purinergic Signal.* **2006**, *2*, 335–341. [[CrossRef](#)]
10. Kim, E.E.; Wyckoff, H.W. Reaction Mechanism of Alkaline Phosphatase Based on Crystal Structures: Two-Metal Ion Catalysis. *J. Mol. Biol.* **1991**, *218*, 449–464. [[CrossRef](#)]
11. Coleman, J.E. Structure and Mechanism of Alkaline Phosphatase. *Annu. Rev. Biophys. Biomol. Struct.* **1992**, *21*, 441–483. [[CrossRef](#)]
12. Hoylaerts, M.F.; Manes, T.; Millán, J.L. Mammalian Alkaline Phosphatases Are Allosteric Enzymes. *J. Biol. Chem.* **1997**, *272*, 22781–22787. [[PubMed](#)]
13. Sligbrand, T. Present Status and Future Trends of Human Alkaline Phosphatases. *Prog Clin Biol Res* **1984**, *166*, 3–14.
14. Harris, H. The Human Alkaline Phosphatases: What We Know and What We Don't Know. *Clin. Chim. Acta* **1990**, *186*, 133–150. [[PubMed](#)]
15. Vincent, J.B.; Crowder, M.W.; Averill, B.A. Hydrolysis of Phosphate Monoesters: A Biological Problem with Multiple Chemical Solutions. *Trends Biochem. Sci.* **1992**, *17*, 105–110.
16. Patel, P.; Mendall, M.A.; Carrington, D.; Strachan, D.P.; Leatham, E.; Molineaux, N.; Levy, J.; Blakeston, C.; Seymour, C.A.; Camm, A.J. Association of Helicobacter Pylori and Chlamydia Pneumoniae Infections with Coronary Heart Disease and Cardiovascular Risk Factors. *BMJ* **1995**, *311*, 711–714. [[CrossRef](#)] [[PubMed](#)]
17. Schepeler, T.; Reinert, J.T.; Ostfeld, M.S.; Christensen, L.L.; Silahatoglu, A.N.; Dyrskjøt, L.; Wiuf, C.; Sørensen, F.J.; Kruhøffer, M.; Laurberg, S. Diagnostic and Prognostic MicroRNAs in Stage II Colon Cancer. *Cancer Res.* **2008**, *68*, 6416–6424. [[PubMed](#)]
18. Lallès, J.-P. Intestinal Alkaline Phosphatase: Novel Functions and Protective Effects. *Nutr. Rev.* **2014**, *72*, 82–94.
19. Hoylaerts, M.F.; Manes, T.; Millán, J.L. Molecular Mechanism of Uncompetitive Inhibition of Human Placental and Germ-Cell Alkaline Phosphatase. *Biochem. J.* **1992**, *286*, 23–30.
20. Giannini, E.G.; Testa, R.; Savarino, V. Liver Enzyme Alteration: A Guide for Clinicians. *Cmaj* **2005**, *172*, 367–379.
21. Ashraf, J.; Mughal, E.U.; Alsantali, R.I.; Sadiq, A.; Jassas, R.S.; Naeem, N.; Ashraf, Z.; Nazir, Y.; Zafar, M.N.; Mumtaz, A. 2-Benzylidenebenzofuran-3 (2 H)-Ones as a New Class of Alkaline Phosphatase Inhibitors: Synthesis, SAR Analysis, Enzyme Inhibitory Kinetics and Computational Studies. *RSC Adv.* **2021**, *11*, 35077–35092. [[CrossRef](#)]
22. Fishman, W.H.; Green, S.; Inglis, N.I. L-Phenylalanine: An Organ Specific, Stereo-Specific Inhibitor of Human Intestinal Alkaline Phosphatase. *Nature* **1963**, *198*, 685–686. [[CrossRef](#)] [[PubMed](#)]
23. Khan, I.; Ibrar, A.; Ejaz, S.A.; Khan, S.U.; Shah, S.J.A.; Hameed, S.; Simpson, J.; Lecka, J.; Sévigny, J.; Iqbal, J. Influence of the Diversified Structural Variations at the Imine Functionality of 4-Bromophenylacetic Acid Derived Hydrazones on Alkaline Phosphatase Inhibition: Synthesis and Molecular Modelling Studies. *RSC Adv.* **2015**, *5*, 90806–90818. [[CrossRef](#)]
24. Miliutina, M.; Ejaz, S.A.; Iaroshenko, V.O.; Villinger, A.; Iqbal, J.; Langer, P. Synthesis of 3, 3'-Carbonyl-Bis (Chromones) and Their Activity as Mammalian Alkaline Phosphatase Inhibitors. *Org. Biomol. Chem.* **2016**, *14*, 495–502. [[CrossRef](#)] [[PubMed](#)]
25. Khan, I.; Shah, S.J.A.; Ejaz, S.A.; Ibrar, A.; Hameed, S.; Lecka, J.; Millán, J.L.; Sévigny, J.; Iqbal, J. Investigation of Quinoline-4-Carboxylic Acid as a Highly Potent Scaffold for the Development of Alkaline Phosphatase Inhibitors: Synthesis, SAR Analysis and Molecular Modelling Studies. *RSC Adv.* **2015**, *5*, 64404–64413. [[CrossRef](#)]
26. Al-Rashida, M.; Iqbal, J. Inhibition of Alkaline Phosphatase: An Emerging New Drug Target. *Mini Rev. Med. Chem.* **2015**, *15*, 41–51. [[CrossRef](#)]
27. Channar, P.A.; Irum, H.; Mahmood, A.; Shabir, G.; Zaib, S.; Saeed, A.; Ashraf, Z.; Larik, F.A.; Lecka, J.; Sevigny, J. Design, Synthesis and Biological Evaluation of Trinary Benzocoumarin-Thiazoles-Azomethines Derivatives as Effective and Selective Inhibitors of Alkaline Phosphatase. *Bioorg. Chem.* **2019**, *91*, 103137. [[CrossRef](#)]
28. Dua, R.; Shrivastava, S.; Sonwane, S.K.; Srivastava, S.K. Pharmacological Significance of Synthetic Heterocycles Scaffold: A Review. *Adv. Biol. Res.* **2011**, *5*, 120–144.
29. Ziarani, G.M.; Nasab, N.H.; Rahimifard, M.; Soorki, A.A. One-Pot Synthesis of Pyrido [2, 3-d] Pyrimidine Derivatives Using Sulfonic Acid Functionalized SBA-15 and the Study on Their Antimicrobial Activities. *J. Saudi Chem. Soc.* **2015**, *19*, 676–681. [[CrossRef](#)]
30. Nasab, N.H.; Safari, J. Synthesis of a Wide Range of Biologically Important Spiropyran and Spiroacenaphthylenes, Using NiFe₂O₄@SiO₂@Melamine Magnetic Nanoparticles as an Efficient, Green and Reusable Nanocatalyst. *J. Mol. Struct.* **2019**, *1193*, 118–124. [[CrossRef](#)]

31. Nasab, N.H.; Safari, J. An Efficient Protocol for the Synthesis of Spiroindenoquinoxaline Derivatives Using Novel NiFe₂O₄/Ag₃PO₄ as a Nano Magnetically Heterogeneous Catalyst. *Polyhedron* **2019**, *164*, 74–79. [[CrossRef](#)]
32. Hosseini Nasab, N.; Han, Y.; Hassan Shah, F.; Vanjare, B.D.; Kim, S.J. Synthesis, Biological Evaluation, Migratory Inhibition and Docking Study of Indenopyrazolones as Potential Anticancer Agents. *Chem. Biodivers.* **2022**, *19*, e202200399. [[CrossRef](#)] [[PubMed](#)]
33. Lv, P.-C.; Sun, J.; Luo, Y.; Yang, Y.; Zhu, H.-L. Design, Synthesis, and Structure–Activity Relationships of Pyrazole Derivatives as Potential FabH Inhibitors. *Bioorg. Med. Chem. Lett.* **2010**, *20*, 4657–4660. [[PubMed](#)]
34. Ragavan, R.V.; Vijayakumar, V.; Kumari, N.S. Synthesis and Antimicrobial Activities of Novel 1, 5-Diaryl Pyrazoles. *Eur. J. Med. Chem.* **2010**, *45*, 1173–1180. [[PubMed](#)]
35. Keter, F.K.; Darkwa, J. Perspective: The Potential of Pyrazole-Based Compounds in Medicine. *Biometals* **2012**, *25*, 9–21. [[CrossRef](#)]
36. Sánchez-Moreno, M.; Gómez-Contreras, F.; Navarro, P.; Marín, C.; Ramírez-Macías, I.; Olmo, F.; Sanz, A.M.; Campayo, L.; Cano, C.; Yunta, M.J.R. In Vitro Leishmanicidal Activity of Imidazole-or Pyrazole-Based Benzo [g] Phthalazine Derivatives against *Leishmania Infantum* and *Leishmania Braziliensis* Species. *J. Antimicrob. Chemother.* **2012**, *67*, 387–397.
37. Jorda, R.; Sacerdoti-Sierra, N.; Voller, J.; Havlíček, L.; Kráčalíková, K.; Nowicki, M.W.; Nasereddin, A.; Kryštof, V.; Strnad, M.; Walkinshaw, M.D. Anti-Leishmanial Activity of Disubstituted Purines and Related Pyrazolo [4, 3-d] Pyrimidines. *Bioorg. Med. Chem. Lett.* **2011**, *21*, 4233–4237.
38. Estevez, Y.; Quiliano, M.; Burguete, A.; Cabanillas, B.; Zimic, M.; Málaga, E.; Verástegui, M.; Pérez-Silanes, S.; Aldana, I.; Monge, A. Trypanocidal Properties, Structure–Activity Relationship and Computational Studies of Quinoxaline 1, 4-Di-N-Oxide Derivatives. *Exp. Parasitol.* **2011**, *127*, 745–751.
39. Fustero, S.; Román, R.; Sanz-Cervera, J.F.; Simón-Fuentes, A.; Bueno, J.; Villanova, S. Synthesis of New Fluorinated Tebufenpyrad Analogs with Acaricidal Activity through Regioselective Pyrazole Formation. *J. Org. Chem* **2008**, *73*, 8545–8552.
40. Sharon, A.; Pratap, R.; Tiwari, P.; Srivastava, A.; Maulik, P.R.; Ram, V.J. Synthesis and in Vivo Antihyperglycemic Activity of 5-(1H-Pyrazol-3-Yl) Methyl-1H-Tetrazoles. *Bioorg. Med. Chem. Lett.* **2005**, *15*, 2115–2117. [[CrossRef](#)]
41. Rosa, F.A.; Machado, P.; Vargas, P.S.; Bonacorso, H.G.; Zanatta, N.; Martins, M.A.P. Straightforward and Regiospecific Synthesis of Pyrazole-5-Carboxylates from Unsymmetrical Enaminodiketones. *Synlett* **2008**, *2008*, 1673–1678.
42. Brown, F.C. 4-Thiazolidinones. *Chem. Rev.* **1961**, *61*, 463–521. [[CrossRef](#)]
43. Song, Y.-X.; Du, D.-M. Recent Advances in the Catalytic Asymmetric Reactions of Thiazolone Derivatives. *Org. Biomol. Chem.* **2020**, *18*, 6018–6041. [[CrossRef](#)] [[PubMed](#)]
44. Dwivedi, C.; Gupta, T.K.; Parmar, S.S. Substituted Thiazolidones as Anticonvulsants. *J. Med. Chem.* **1972**, *15*, 553–554. [[CrossRef](#)] [[PubMed](#)]
45. Chaudhary, M.; Parmar, S.S.; Chaudhary, S.K.; Chaturvedi, A.K.; Sastry, B.V.R. CNS Depressant Activity of Pyrimidylthiazolidones and Their Selective Inhibition of NAD-dependent Pyruvate Oxidation. *J. Pharm. Sci.* **1976**, *65*, 443–446. [[CrossRef](#)] [[PubMed](#)]
46. Babaoglu, K.; Page, M.A.; Jones, V.C.; McNeil, M.R.; Dong, C.; Naismith, J.H.; Lee, R.E. Novel Inhibitors of an Emerging Target in *Mycobacterium Tuberculosis*; Substituted Thiazolidinones as Inhibitors of DTDP-Rhamnose Synthesis. *Bioorg. Med. Chem. Lett.* **2003**, *13*, 3227–3230. [[CrossRef](#)]
47. Kavitha, C.V.; Swamy, S.N.; Mantelingu, K.; Doreswamy, S.; Sridhar, M.A.; Prasad, J.S.; Rangappa, K.S. Synthesis of New Bioactive Venlafaxine Analogs: Novel Thiazolidin-4-Ones as Antimicrobials. *Bioorg. Med. Chem.* **2006**, *14*, 2290–2299. [[CrossRef](#)]
48. Gududuru, V.; Hurh, E.; Dalton, J.T.; Miller, D.D. Synthesis and Antiproliferative Activity of 2-Aryl-4-Oxo-Thiazolidin-3-Yl-Amides for Prostate Cancer. *Bioorg. Med. Chem. Lett.* **2004**, *14*, 5289–5293. [[CrossRef](#)]
49. Fu, J.-Y.; Masferrer, J.L.; Seibert, K.; Raz, A.; Needleman, P. The Induction and Suppression of Prostaglandin H₂ Synthase (Cyclooxygenase) in Human Monocytes. *J. Biol. Chem.* **1990**, *265*, 16737–16740. [[CrossRef](#)]
50. Havrylyuk, D.; Roman, O.; Lesyk, R. Synthetic Approaches, Structure Activity Relationship and Biological Applications for Pharmacologically Attractive Pyrazole/Pyrazoline–Thiazolidine-Based Hybrids. *Eur. J. Med. Chem.* **2016**, *113*, 145–166. [[CrossRef](#)]
51. Yuan, J.; Yuan, C.; Degterev, A. Unsaturated Heterocyclic Inhibitors of Necroptosis. WO2010075290A1, 2010.
52. Mustelin, T.; Tautz, L. VHR Protein Tyrosine Phosphatase Inhibitors, Compositions and Methods of Use. US20090105254, 2012.
53. Bao, L.; Kimzey, A. Pin1-Modulating Compounds and Methods of Use for the Treatment of Pin1-Associated Diseases, Including Cancer. WO 2004093803, 2004.
54. Ryder, S. Compounds for Modulating Rna Binding Proteins and Uses Therefor. WO 2010151799, 2011.
55. Carter, P.H.; Scherle, P.A.; Muckelbauer, J.A.; Voss, M.E.; Liu, R.-Q.; Thompson, L.A.; Tebben, A.J.; Solomon, K.A.; Lo, Y.C.; Li, Z. Photochemically Enhanced Binding of Small Molecules to the Tumor Necrosis Factor Receptor-1 Inhibits the Binding of TNF- α . *Proc. Natl. Acad. Sci. USA* **2001**, *98*, 11879–11884. [[CrossRef](#)]
56. Furdas, S.D.; Shekfeh, S.; Kannan, S.; Sippl, W.; Jung, M. Rhodanine Carboxylic Acids as Novel Inhibitors of Histone Acetyltransferases. *Medchemcomm* **2012**, *3*, 305–311. [[CrossRef](#)]
57. Qiu, K.-M.; Yan, R.; Xing, M.; Wang, H.-H.; Cui, H.-E.; Gong, H.-B.; Zhu, H.-L. Synthesis, Biological Evaluation and Molecular Modeling of Dihydro-Pyrazolyl-Thiazolinone Derivatives as Potential COX-2 Inhibitors. *Bioorg. Med. Chem.* **2012**, *20*, 6648–6654. [[CrossRef](#)] [[PubMed](#)]
58. Gilbert, A.M.; Bursavich, M.G.; Lombardi, S.; Georgiadis, K.E.; Reifenberg, E.; Flannery, C.R.; Morris, E.A. 5-((1H-Pyrazol-4-Yl) Methylene)-2-Thioxothiazolidin-4-One Inhibitors of ADAMTS-5. *Bioorg. Med. Chem. Lett.* **2007**, *17*, 1189–1192. [[CrossRef](#)]
59. Kadam, R.U.; Roy, N. Recent Trends in Drug-Likeness Prediction: A Comprehensive Review of in Silico Methods. *Indian J. Pharm. Sci.* **2007**, *69*, 609–615.

60. Hassan, M.; Abbasi, M.A.; Siddiqui, S.Z.; Hussain, G.; Shah, S.A.A.; Shahid, M.; Seo, S.-Y. Exploration of Synthetic Multifunctional Amides as New Therapeutic Agents for Alzheimer's Disease through Enzyme Inhibition, Chemoinformatic Properties, Molecular Docking and Dynamic Simulation Insights. *J. Theor. Biol.* **2018**, *458*, 169–183. [[CrossRef](#)]
61. Bakht, M.A.; Yar, M.S.; Abdel-Hamid, S.G.; Al Qasoumi, S.I.; Samad, A. Molecular Properties Prediction, Synthesis and Antimicrobial Activity of Some Newer Oxadiazole Derivatives. *Eur. J. Med. Chem.* **2010**, *45*, 5862–5869. [[CrossRef](#)]
62. Tian, S.; Wang, J.; Li, Y.; Li, D.; Xu, L.; Hou, T. The Application of in Silico Drug-Likeness Predictions in Pharmaceutical Research. *Adv. Drug Deliv. Rev.* **2015**, *86*, 2–10. [[CrossRef](#)]
63. Charifson, P.S.; Corkery, J.J.; Murcko, M.A.; Walters, W.P. Consensus Scoring: A Method for Obtaining Improved Hit Rates from Docking Databases of Three-Dimensional Structures into Proteins. *J. Med. Chem.* **1999**, *42*, 5100–5109. [[CrossRef](#)] [[PubMed](#)]
64. Iqbal, Z.; Iqbal, A.; Ashraf, Z.; Latif, M.; Hassan, M.; Nadeem, H. Synthesis and Docking Studies of N-(5-(Alkylthio)-1, 3, 4-oxadiazol-2-yl) Methyl) Benzamide Analogues as Potential Alkaline Phosphatase Inhibitors. *Drug Dev. Res.* **2019**, *80*, 646–654. [[CrossRef](#)] [[PubMed](#)]
65. Saeed, A.; Saddique, G.; Channar, P.A.; Larik, F.A.; Abbas, Q.; Hassan, M.; Raza, H.; Fattah, T.A.; Seo, S.-Y. Synthesis of Sulfadiazinyl Acyl/Aryl Thiourea Derivatives as Calf Intestinal Alkaline Phosphatase Inhibitors, Pharmacokinetic Properties, Lead Optimization, Lineweaver-Burk Plot Evaluation and Binding Analysis. *Bioorg. Med. Chem.* **2018**, *26*, 3707–3715.
66. Özdemir, A.; Sever, B.; Altıntop, M.D.; Kaya Tilki, E.; Dikmen, M. Design, Synthesis, and Neuroprotective Effects of a Series of Pyrazolines against 6-Hydroxydopamine-Induced Oxidative Stress. *Molecules* **2018**, *23*, 2151. [[CrossRef](#)]
67. Altıntop, M.D.; Özdemir, A.; Turan-Zitouni, G.; Ilgın, S.; Atlı, Ö.; Demirel, R.; Kaplancıklı, Z.A. A Novel Series of Thiazolyl-Pyrazoline Derivatives: Synthesis and Evaluation of Antifungal Activity, Cytotoxicity and Genotoxicity. *Eur. J. Med. Chem.* **2015**, *92*, 342–352. [[CrossRef](#)] [[PubMed](#)]
68. Abbasi, M.A.; Nazir, M.; Siddiqui, S.Z.; Raza, H.; Zafar, A.; Shah, S.A.A.; Shahid, M. Synthesis, In Vitro, and In Silico Studies of N-(Substituted-Phenyl)-3-(4-Phenyl-1-Piperazinyl) Propanamides as Potent Alkaline Phosphatase Inhibitors. *Russ. J. Bioorganic Chem.* **2021**, *47*, 1086–1096. [[CrossRef](#)]
69. Berkman, S.J.; Roscoe, E.M.; Bourret, J.C. Comparing Self-directed Methods for Training Staff to Create Graphs Using Graphpad Prism. *J. Appl. Behav. Anal.* **2019**, *52*, 188–204. [[PubMed](#)]
70. Abbasi, M.A.; Nazir, M.; ur-Rehman, A.; Siddiqui, S.Z.; Hassan, M.; Raza, H.; Shah, S.A.A.; Shahid, M.; Seo, S. Bi-heterocyclic Benzamides as Alkaline Phosphatase Inhibitors: Mechanistic Comprehensions through Kinetics and Computational Approaches. *Arch. Pharm. (Weinheim)* **2019**, *352*, 1800278. [[CrossRef](#)]
71. Abbas, Q.; Ashraf, Z.; Hassan, M.; Nadeem, H.; Latif, M.; Afzal, S.; Seo, S.-Y. Development of Highly Potent Melanogenesis Inhibitor by in Vitro, in Vivo and Computational Studies. *Drug Des. Devel. Ther.* **2017**, *11*, 2029.
72. Pettersen, E.F.; Goddard, T.D.; Huang, C.C.; Couch, G.S.; Greenblatt, D.M.; Meng, E.C.; Ferrin, T.E. UCSF Chimera—A Visualization System for Exploratory Research and Analysis. *J. Comput. Chem.* **2004**, *25*, 1605–1612. [[CrossRef](#)] [[PubMed](#)]
73. Discovery, S. DS Visualizer and ActiveX Control 2008.
74. Willard, L.; Ranjan, A.; Zhang, H.; Monzavi, H.; Boyko, R.F.; Sykes, B.D.; Wishart, D.S. VADAR: A Web Server for Quantitative Evaluation of Protein Structure Quality. *Nucleic Acids Res.* **2003**, *31*, 3316–3319. [[CrossRef](#)] [[PubMed](#)]
75. Dallakyan, S.; Olson, A.J. Small-Molecule Library Screening by Docking with PyRx. In *Chemical Biology*; Springer: Berlin/Heidelberg, Germany, 2015; pp. 243–250.
76. Gottlieb, H.E.; Kotlyar, V.; Nudelman, A. NMR chemical shifts of common laboratory solvents as trace impurities. *J. Org. Chem.* **1997**, *62*, 7512–7515. [[CrossRef](#)] [[PubMed](#)]